CrystEngComm

Dynamic Article Links

Cite this: *CrystEngComm*, 2012, **14**, 7981–7993

www.rsc.org/crystengcomm

PAPER

Novel 1-D double-chain organic–inorganic hybrid polyoxotungstates constructed from dimeric copper–lanthanide heterometallic silicotungstate units†

Junwei Zhao,*[ab] Jie Luo,[ac] Lijuan Chen,*[ac] Jing Yuan,[a] Huiying Li,[a] Pengtao Ma,[a] Jingping Wang[a] and Jingyang Niu*[a]

Received 23rd June 2012, Accepted 22nd August 2012
DOI: 10.1039/c2ce26007g

A series of novel 1-D double-chain organic–inorganic hybrid polyoxotungstates $[Cu(dap)_2(H_2O)]_2\{Cu(dap)_2[\alpha\text{-}H_2SiW_{11}O_{39}Ln(H_2O)_3]_2\}\cdot xH_2O$ [Ln = Ce^{III}, x = 9 (**1**); Ln = Pr^{III}, x = 10 (**2**), Ln = Nd^{III}, x = 10 (**3**), Ln = Sm^{III}, x = 10 (**4**), Ln = Eu^{III}, x = 10 (**5**), Ln = Gd^{III}, x = 9 (**6**), Ln = Tb^{III}, x = 8 (**7**), Ln = Dy^{III}, x = 8 (**8**), Ln = Er^{III}, x = 9 (**9**)] (dap = 1,2-diaminopropane) have been hydrothermally prepared and structurally characterized by elemental analyses, inductively coupled plasma atomic emission spectrometry, IR spectra, UV-Vis spectra, thermogravimetric analyses and single-crystal X-ray diffraction. Compounds **1–9** are isomorphic and display the novel 1-D double-chain built by dimeric copper–lanthanide heterometallic silicotungstate units by means of the bridging role of the lanthanide cations, to our knowledge, which represent the first organic–inorganic hybrid 1-D double-chain copper–lanthanide heterometallic polyoxometalates. The variable-temperature magnetic susceptibilities of **2**, **3**, **6** and **8** have been investigated. The solid-state photoluminescence properties of **4**, **5**, **7** and **8** have been measured at room temperature.

Introduction

The continuous interest in exploring and discovering novel transition-metal (TM) or lanthanide (Ln) substituted polyoxometalates (POMs) has persisted owing not only to the diversity in their molecular structures and properties but also to their applications in catalysis, medicine, magnetism, photochemistry, conduction and materials science.[1] The self-assembly is usually the most useful strategy in synthesizing novel POMs, in which large structures can be constructed *via* condensation steps thermodynamically driven by charge and nucleophilicity of the *in situ* formed transient cluster fragments.[1a] Lacunary POM fragments integrating various TM or Ln metal ions have proved this approach and have led to a rich class of TM or Ln substituted POMs.[2] With the rapid development of POM chemistry and the interpenetrating trend of multidisciplinarities, recently, the synthesis and exploitation of POM-based TM–Ln heterometallic derivatives (PTLHDs) have gradually become a challenging area. Since the first PTLHD $[((VO)_2Dy(H_2O)_4K_2(H_2O)_2Na(H_2O)_2)(B\text{-}\alpha\text{-}AsW_9O_{33})_2]^{8-}$ was discovered by Müller *et al.* in 2007,[3] only a small number of PTLHDs have been obtained mainly because there exists an unavoidable competitive reaction among highly negative POM precursors, strongly oxyphilic Ln metal cations and less active TM cations in the same reaction system.[4] Some typical research findings are listed here: Kögerler'group reported two novel Dawson-type phosphotungstate-based Ce^{IV}–Mn^{IV} heterometallic clusters $[\{\alpha\text{-}P_2W_{15}O_{56}\}_6\{Ce_3Mn_2(\mu_3\text{-}O)_4(\mu_2\text{-}OH)_2\}_3(\mu_2\text{-}OH)_2(H_2O)_2(PO_4)]^{47-}$,[5a] and $[\{\alpha\text{-}P_2W_{16}O_{57}(OH)_2\}\{CeMn_6O_9(O_2CCH_3)_8\}]^{8-}$;[5b] Wang's group prepared several classes of intriguing PTLHDs such as 1-D chiral ladder-like chain $[\{Ce(H_2O)_7\}_2Mn_4Si_2W_{18}O_{68}(H_2O)_2]^{6-}$,[5c] a trimeric $[K\subset\{FeCe(AsW_{10}O_{38})(H_2O)_2\}_3]^{14-}$,[4] two $\{P_2W_{12}\}$-based $[K_3\subset\{GdMn(H_2O)_{10}\}\{HMnGd_2(Tart)O_2(H_2O)_{15}\}\{P_6W_{42}O_{151}(H_2O)_7\}]^{11-}$,[5d] and $[K_3\subset\{GdCo(H_2O)_{11}\}_2\{P_6W_{41}O_{148}(H_2O)_7\}]^{13-}$,[5d] one triple-Dawson-type $\{[Ce_3Mn_2O_6(OAc)_6(H_2O)_9]_2[Mn_2P_2W_{16}O_{60}]_3\}^{20-}$,[5e] and two hexameric $[K_9Ln_6Fe_6(H_2O)_{12}(SiW_{10}O_{38})_6]^{26-}$ (Ln = Dy^{III}, Tb^{III});[5f] Mialane's group communicated a family of $\{LnCu_3(OH)_3O\}$-cubane-containing $\{[Cu(en)_2(H_2O)][(Cu(en)(OH))_3Ln(SiW_{11}O_{39})(H_2O)]\}_2\cdot 20H_2O$ (Ln = La^{III}, Gd^{III}, Eu^{III}),[5g] and a double-chain monodimensional $[(\gamma\text{-}SiW_{10}O_{36})_2(Cr(OH)(H_2O))_3(La(H_2O)_7)_2]^{4-}$;[5h] Liu *et al.* addressed a family of 1D $[\{Ln(PW_{11}O_{39})_2\}\{Cu_2(bpy)_2(\mu\text{-}ox)\}]^{9-}$ (Ln = La^{III}, Pr^{III}, Eu^{III}, Gd^{III}, Yb^{III}); [5i] Reinoso *et al.* synthesized a sandwich-type $[\{Ce(H_2O)_2\}_2Mn_2(B\text{-}\alpha\text{-}GeW_9O_{34})_2]^{8-}$,[5j] and a giant crown-shaped $[K\subset K_7Ce_{24}Ge_{12}W_{120}O_{456}(OH)_{12}(H_2O)_{64}]^{52-}$,[5k]

[a]*Institute of Molecular and Crystal Engineering, College of Chemistry and Chemical Engineering, Henan University, Kaifeng, Henan 475004, P. R. China. E-mail: zhaojunwei@henu.edu.cn; jyniu@henu.edu.cn; Fax: (+86) 378 3886876*
[b]*State Key Laboratory of Structural Chemistry, Fujian Institute of Research on the Structure of Matter, Chinese Academy of Sciences, Fuzhou, Fujian 350002, P. R. China*
[c]*Basic Experiment Teaching Center, Henan University, Kaifeng, Henan 475004, P. R. China*

† Electronic Supplementary Information (ESI) available: Additional data. CCDC reference numbers 876154–876162 for **1–9**. For ESI and crystallographic data in CIF or other electronic format see DOI: 10.1039/c2ce26007g

moreover, he reviewed the advance of PTLHDs; [5l] Our group isolated several types of PTLHDs including $[Cu(en)_2]_{1.5}[Cu(en)(2,2'\text{-bipy})]Ce[(\alpha\text{-}PW_{11}O_{39})_2]\}^{6-}$,[5m] $\{[Cu(en)_2]_2(H_2O)[Cu(en)(2,2'\text{-bipy})]Ln[(\alpha\text{-}HPW_{11}O_{39})_2]\}^{4-}$ (Ln = Gd^{III}, Tb^{III}, Er^{III}),[5m] $\{[(\alpha\text{-}PW_{11}O_{39})Ln(H_2O)]_2(C_2O_4)\}^{10-}$ (Ln = Y^{III}, Dy^{III}, Ho^{III}, Er^{III}),[5n] $\{(\alpha\text{-}x\text{-}PW_{10}O_{38})Tm_2(C_2O_4)(H_2O)_2\}^{3-}$,[5n] $\{[Cu(en)_2]_{1.5}Ln[(\alpha\text{-}SiW_{11}O_{39})_2]\}_2^{20-}$ (Ln = Gd^{III}, Tb^{III}, Dy^{III}, Er^{III}, Lu^{III}),[5o] $\{[Cu(en)_2]_{1.5}Ln[(\alpha\text{-}SiW_{11}O_{39})]\}^{2-}$ (Ln = La^{III}, Ce^{III}),[5o] $[Cu(en)_2(H_2O)][Cu(en)_2]_{1.5}[H_3Ln(\alpha\text{-}AsW_{11}O_{39})_2]^{3-}$ (Ln = Pr^{III}, Nd^{III}, Sm^{III}, Eu^{III}, Tb^{III}),[5p] $[Cu(dap)_2]_{5.5}[Ln(\alpha\text{-}AsW_{11}O_{39})_2]\cdot xH_2O$ (Ln = Tb^{III}, x = 6; Ln = Dy^{III}, x = 5),[5p] and $[Cu(en)_2(H_2O)]_2\{[Cu(en)_2][Cu(en)_2(H_2O)][(\alpha\text{-}SiW_{11}O_{39})Ln(H_2O)(pzda)]\}_2^{2-}$ (Ln = Y^{III}, Dy^{III}, Yb^{III}, Lu^{III}). [5q] From the above we can see that the reports on silicotungstate-based TM–Ln heterometallic derivatives are very sporadic,[5c,f,g,h,o,q] most of which were prepared by the reaction of plenary, monovacant or divacant Keggin-type silicotungstate precursors with TM–Ln cations. However, investigations on the system containing trivacant Keggin-type silicotungstate precursors, TM cations and Ln cations remain rarer,[5g] which provides great interest and an excellent opportunity. The current trend is towards "rational design" based on the accumulated knowledge of crystal chemistry, thermodynamics and reactivity as well as the relationship between structures and properties.[6] As a part of our continuous work, recently, we have initiated exploitation of the reactions of the trivacant Keggin-type $[A\text{-}\alpha\text{-}SiW_9O_{34}]^{10-}$ precursor with copper and Ln cations in the participation of organic components under hydrothermal conditions based on the following considerations. (a) The trivacant Keggin-type $[A\text{-}\alpha\text{-}SiW_9O_{34}]^{10-}$ precursor is easily prepared in a one-step process with high yield, which provides us with abundant initial material to made novel PTLHDs with unexpected structures and properties under hydrothermal conditions, and this precursor can transform and isomerize to $[B\text{-}\alpha\text{-}SiW_9O_{34}]^{10-}$, $[\alpha\text{-}SiW_{11}O_{39}]^{8-}$, $[\alpha\text{-}SiW_{12}O_{40}]^{4-}$ and $[\beta\text{-}SiW_8O_{31}]^{10-}$ intermediate phases during the course of the reaction, offering greater possibilities to simultaneously capture copper and Ln metal cations. (b) Compared with other TM cations, the copper ions display flexible various coordination geometries (trigonal bipyramid, square pyramid and octahedron) and the obvious Jahn–Teller effect and pseudo–Jahn–Teller effect, which are rather favorable for combining with the *in situ* generated silicotungstate intermediate phases, moreover, the oxophilicity and multiple coordination requirementsof Ln cations also benefit this point. (c) Previous studies suggest that organic N-ligands are good donors to chelate electrophilic copper cations forming metal–organic complexes, which often function as the connectors to construct extended architectures,[6,7] as a result, 1,2-diaminopropane (dap) has been selected. (d) Because the reactions of oxyphilic Ln cations with lacunary silicotungstate precursors usually result in precipitation, leading to their lower reactive activity, the hydrothermal technique has been employed to enhance the solubility of silicotungstate precursors, copper cations, Ln cations and organic components in the reaction system and make the reaction shift from the thermodynamic to the kinetic so that the equilibrium phases are replaced by structurally more complicated metastable phases.[8] Under the guidance of these ideas, we have successfully synthesized nine novel 1-D double-chain PTLHD hybrids $[Cu(dap)_2(H_2O)]_2\{Cu(dap)_2[\alpha\text{-}H_2SiW_{11}O_{39}Ln(H_2O)_3]_2\}\cdot x\,H_2O$ [Ln = Ce^{III}, x = 9 (**1**); Ln = Pr^{III}, x = 10 (**2**), Ln = Nd^{III}, x = 10 (**3**), Ln = Sm^{III}, x = 10 (**4**), Ln = Eu^{III}, x = 10 (**5**), Ln = Gd^{III}, x = 9 (**6**), Ln = Tb^{III}, x = 8 (**7**), Ln = Dy^{III}, x = 8 (**8**), Ln = Er^{III}, x = 9 (**9**)] (dap = 1,2-diaminopropane), which illustrate the novel 1-D double-chain motifs constructed by dimeric Cu–Ln heterometallic silicotungstate units through Ln cations. As far as we know, they are the first organic–inorganic hybrid 1-D double-chain PTLHDs. Moreover, the synthetic conditions of the reported silicotungstate-based TM–Ln heterometallic derivatives have been summarized. The magnetic behavior of **2** and **3** is intimately related to the depopulation of the Stark levels upon cooling while the magnetic behavior of **6** and **8** at the higher temperature region may indicate that the S_{Gd} = 7/2 or S_{Dy} = 5/2 local spins somewhat tend to align along the same direction and a sudden decrease of the $\chi_M T$ value below 17 K or 34 K can be ascribed to the intermolecular antiferromagnetic interactions. The luminescence properties of **4**, **5**, **7** and **8** have been examined and their luminescence primarily originates from the nature of Ln cations. The thermogravimetric curves of **2**, **3**, **5**, **6**, **7** and **8** indicate two steps of weight loss.

Experimental

Materials and physical measurements

The trilacunary precursor $Na_{10}[A\text{-}\alpha\text{-}SiW_9O_{34}]\cdot 18H_2O$ was synthesized as previously described[9] and further identified by IR spectra. All other reagents were used as purchased without further purification. Elemental analyses (C, H and N) were performed on a Perkin–Elmer 2400–II CHNS/O analyzer. Inductively coupled plasma atomic emission spectrometry (ICP–AES) was performed on a Perkin–Elmer Optima 2000 ICP–AES spectrometer. IR spectra were recorded on a Nicolet FT-IR 360 spectrometer using KBr pellets in the range of 4000–400 cm^{-1}. UV-Vis spectra were obtained on a HITACHI U–4100 UV–Vis–NIR spectrometer at room temperature. Emission/excitation spectra were recorded on a HITACHI F–7000 fluorescence spectrophotometer. Thermogravimetric analyses were performed under a N_2 atmosphere on a Mettler–Toledo TGA/SDTA851^e instrument with a heating rate of 10 °C min^{-1} from 25 to 750 °C. Variable-temperature magnetic susceptibility measurements were carried out in the temperature range of 2.7–300 K on a Quantum Design MPMS–5 SQUID magnetometer in an applied magnetic field of 2000 Oe. Experimental susceptibilities were corrected for diamagnetism of the constituent atoms by use of Pascal's constants.

Preparation of 1–9

$[Cu(dap)_2(H_2O)]_2\{Cu(dap)_2[\alpha\text{-}H_2SiW_{11}O_{39}Ce(H_2O)_3]_2\}\cdot 9\,H_2O$ (1). A mixture of $Na_{10}[A\text{-}\alpha\text{-}SiW_9O_{34}]\cdot 18H_2O$ (0.170 g, 0.061 mmol), $CuCl_2\cdot 2H_2O$ (0.140 g, 0.821 mmol), $Ce(NO_3)_3\cdot 6H_2O$ (0.083 g, 0.191 mmol), dap (0.15 mL, 1.767 mmol), H_2O (6 mL, 333 mmol) and HCl (0.30 mL, 2 mol L^{-1}) was stirred for 3 h, sealed in a 25 mL Teflon-lined steel autoclave, kept at 160 °C for 6 days and then cooled to room temperature. Brownish block crystals were obtained by filtering, washed with distilled water and dried in air at ambient temperature. Yield: *ca.* 31% (based on $Na_{10}[A\text{-}\alpha\text{-}SiW_9O_{34}]\cdot 18H_2O$). Anal. Calcd. (found%) for $C_{18}H_{98}N_{12}O_{95}Cu_3Ce_2Si_2W_{22}$ (**1**): C 3.29 (3.38), H 1.50 (1.63), N 2.56 (2.49), Cu 2.90 (2.82), Ce 4.26 (4.37), Si 0.85 (0.89), W 61.52 (61.70). IR (KBr pellets, cm^{-1}): 3464(vs), 3300(w), 3252(w), 3138(w), 2967(w),

2886(w), 1629(m), 1588(m), 1460(w), 1385(w), 1175(w), 1065(m), 997(m), 948(s), 889(vs), 821(vs), 780(vs), 699(s), 536(m) (Fig. S1).

$[Cu(dap)_2(H_2O)]_2\{Cu(dap)_2[\alpha\text{-}H_2SiW_{11}O_{39}Pr(H_2O)_3]_2\}\cdot 10H_2O$ (2). A mixture of $Na_{10}[A\text{-}\alpha\text{-}SiW_9O_{34}]\cdot 18H_2O$ (0.125 g, 0.045 mmol), $CuCl_2\cdot 2H_2O$ (0.140 g, 0.821 mmol), $PrCl_3$ (0.048 g, 0.194 mmol), dap (0.10 mL, 1.178 mmol), H_2O (4 mL, 222 mmol) and HCl (0.15 mL, 2 mol L^{-1}) was stirred for 3 h, sealed in a 25 mL Teflon-lined steel autoclave, heated at 160 °C for 6 days and then cooled to room temperature. Purple prismatic crystals were separated by filtering, washed with distilled water and dried in air. Yield: *ca.* 25% (based on $Na_{10}[A\text{-}\alpha\text{-}SiW_9O_{34}]\cdot 18H_2O$). Anal. Calcd. (found%) for $C_{18}H_{100}N_{12}O_{96}Cu_3Pr_2Si_2W_{22}$ (**2**): C 3.28 (3.35), H 1.53 (1.68), N 2.55 (2.61), Cu 2.89 (2.95), Pr 4.27 (4.14), Si 0.85 (0.78), W 61.33 (61.43). IR (KBr pellets, cm^{-1}): 3470(vs), 3307(w), 3252(w), 3138(w), 2960(w), 2879(w), 1622(m), 1581(m), 1460(w), 1386(w), 1177(w), 1066(m), 997(m), 943 (s), 887(vs), 821(vs), 775(vs), 705(s), 536(m) (Fig. S1).

$[Cu(dap)_2(H_2O)]_2\{Cu(dap)_2[\alpha\text{-}H_2SiW_{11}O_{39}Nd(H_2O)_3]_2\}\cdot 10H_2O$ (3). The synthetic procedure was identical to 2, we used $Na_{10}[A\text{-}\alpha\text{-}SiW_9O_{34}]\cdot 18H_2O$ (0.135 g, 0.049 mmol) and $NdCl_3$ (0.049 g, 0.196 mmol) in place of $Na_{10}[A\text{-}\alpha\text{-}SiW_9O_{34}]\cdot 18H_2O$ (0.125 g, 0.045 mmol) and $PrCl_3$ (0.048 g, 0.194 mmol). Purple prismatic crystals were afforded. Yield: *ca.* 26% (based on $Na_{10}[A\text{-}\alpha\text{-}SiW_9O_{34}]\cdot 18H_2O$). Anal. Calcd. (found%) for $C_{18}H_{100}N_{12}O_{96}Cu_3Nd_2Si_2W_{22}$ (**3**): C 3.28 (3.20), H 1.53 (1.70), N 2.55 (2.49), Cu 2.89 (2.78), Nd 4.37 (4.42), Si 0.85 (0.79), W 61.27 (61.17). IR (KBr pellets, cm^{-1}): 3470(vs), 3300(w), 3252(w), 3138(w), 2967(w), 2886(w), 1622(m), 1582(m), 1453(w), 1385(w), 1175(w), 1066(m), 993 (m), 943(s), 889(vs), 828(vs), 780(vs), 704(s), 535(m) (Fig. S1).

$[Cu(dap)_2(H_2O)]_2\{Cu(dap)_2[\alpha\text{-}H_2SiW_{11}O_{39}Sm(H_2O)_3]_2\}\cdot 10H_2O$ (4). A mixture of $Na_{10}[A\text{-}\alpha\text{-}SiW_9O_{34}]\cdot 18H_2O$ (0.130 g, 0.047 mmol), $CuCl_2\cdot 2H_2O$ (0.140 g, 0.821 mmol), $SmCl_3$ (0.050 g, 0.195 mmol), dap (0.20 mL, 2.356 mmol), H_2O (5 mL, 278 mmol) and HCl (0.30 mL, 2 mol L^{-1}) was stirred for 3 h, sealed in a 25 mL Teflon-lined steel autoclave, heated at 160 °C for 6 days and then cooled to room temperature. Purple prismatic crystals were separated by filtration, washed with distilled water and dried in air. Yield: *ca.* 29% (based on $Na_{10}[A\text{-}\alpha\text{-}SiW_9O_{34}]\cdot 18H_2O$). Anal. Calcd. (found%) for $C_{18}H_{100}N_{12}O_{96}Cu_3Sm_2Si_2W_{22}$ (**4**): C 3.27 (3.33), H 1.52 (1.67), N 2.54 (2.61), Cu 2.88 (2.80), Sm 4.55 (4.45), Si 0.85 (0.90), W 61.16 (61.08). IR (KBr pellets, cm^{-1}): 3466(vs), 3305(w), 3252(w), 3137(w), 2961(w), 2880(w), 1623(m), 1582(m), 1455(w), 1385(w), 1170(w), 1065(m), 995(m), 943 (s), 889(vs), 821(vs), 778(vs), 705(s), 533(m) (Fig. S1).

$[Cu(dap)_2(H_2O)]_2\{Cu(dap)_2[\alpha\text{-}H_2SiW_{11}O_{39}Eu(H_2O)_3]_2\}\cdot 10H_2O$ (5). The procedure for the formation of **1** was employed, but the amount of $Na_{10}[A\text{-}\alpha\text{-}SiW_9O_{34}]\cdot 18H_2O$ was changed to (0.150 g, 0.054 mmol) and $Ce(NO_3)_3\cdot 6H_2O$ was replaced by $EuCl_3$ (0.050 g, 0.194 mmol). Purple prismatic crystals were obtained Yield: *ca.* 36% (based on $Na_{10}[A\text{-}\alpha\text{-}SiW_9O_{34}]\cdot 18H_2O$). Anal. Calcd. (found%) for $C_{18}H_{100}N_{12}O_{96}Cu_3Eu_2Si_2W_{22}$ (**5**): C 3.27 (3.12), H 1.52 (1.71), N 2.54 (2.58), Cu 2.88 (2.77), Eu 4.59 (4.66), Si 0.85 (0.79), W 61.13 (61.22). IR (KBr pellets, cm^{-1}): 3466(vs), 3301(w), 3252(w), 3138(w), 2967(w), 2880(w), 1622(m), 1587(m), 1460(w), 1391(w), 1175(w), 1066(m), 997(m), 944(s), 889 (vs), 820(vs), 780(vs), 703(s), 535(m) (Fig. S1).

$[Cu(dap)_2(H_2O)]_2\{Cu(dap)_2[\alpha\text{-}H_2SiW_{11}O_{39}Gd(H_2O)_3]_2\}\cdot 9H_2O$ (6). Similar to the procedure of **2**, but $GdCl_3$ (0.051 g, 0.190 mmol) was used instead of $PrCl_3$. The amounts of dap and HCl were changed to (0.20 mL, 2.356 mmol) and (0.30 mL, 2 mol L^{-1}), respectively. After 5 days, purple prismatic crystals were obtained. Yield: *ca.* 22% (based on $Na_{10}[A\text{-}\alpha\text{-}SiW_9O_{34}]\cdot 18H_2O$). Anal. Calcd. (found%) for $C_{18}H_{98}N_{12}O_{95}Cu_3Gd_2Si_2W_{22}$ (**6**): C 3.27 (3.12), H 1.49 (1.54), N 2.54 (2.46), Cu 2.88 (2.96), Gd 4.76 (4.68), Si 0.85 (0.77), W 61.20 (61.31). IR (KBr pellets, cm^{-1}): 3469(vs), 3301(w), 3253(w), 3137(w), 2963(w), 2878(w), 1622(m), 1582(m), 1458(w), 1385(w), 1176(w), 1066(m), 997(m), 943(s), 883(vs), 821(vs), 780(vs), 706(s), 535(m) (Fig. S1).

$[Cu(dap)_2(H_2O)]_2\{Cu(dap)_2[\alpha\text{-}H_2SiW_{11}O_{39}Tb(H_2O)_3]_2\}\cdot 8H_2O$ (7). **7** was prepared according to the method of **5**, but $TbCl_3$ (0.051 g, 0.192 mmol) was used instead of $EuCl_3$. Purple prismatic crystals were obtained. Yield: *ca.* 28% (based on $Na_{10}[A\text{-}\alpha\text{-}SiW_9O_{34}]\cdot 18H_2O$). Anal. Calcd. (found%) for $C_{18}H_{96}N_{12}O_{94}Cu_3\ Si_2Tb_2W_{22}$ (**7**): C 3.28 (3.37), H 1.47 (1.60), N 2.55 (2.63), Cu 2.89 (2.81), Tb 4.82 (4.94), Si 0.85 (0.91), W 61.33 (61.27). IR (KBr pellets, cm^{-1}): 3470(vs), 3301(w), 3252(w), 3137(w), 2966(w), 2879(w), 1623(m), 1581(m), 1455(w), 1390(w), 1170(w), 1065(m), 997(m), 943(s), 885(vs), 821(vs), 778(vs), 704(s), 530(m) (Fig. S1).

$[Cu(dap)_2(H_2O)]_2\{Cu(dap)_2[\alpha\text{-}H_2SiW_{11}O_{39}Dy(H_2O)_3]_2\}\cdot 8H_2O$ (8). **8** was prepared similar to **6**, but $DyCl_3$ (0.053 g, 0.197 mmol) was used instead of $GdCl_3$. Purple prismatic crystals were afforded. Yield: *ca.* 25% (based on $Na_{10}[A\text{-}\alpha\text{-}SiW_9O_{34}]\cdot 18H_2O$). Anal. Calcd. (found%) for $C_{18}H_{96}Cu_3Dy_2N_{12}O_{94}Si_2W_{22}$ (**8**): C 3.28 (3.20), H 1.47 (1.58), N 2.55 (2.46), Cu 2.89 (2.97), Dy 4.92 (4.80), Si 0.85 (0.76), W 61.27 (61.09). IR (KBr pellets, cm^{-1}): 3476(vs), 3306(w), 3251(w), 3137(w), 2967(w), 2886(w), 1629(m), 1582(m), 1460(w), 1385(w), 1168(w), 1066(m), 998 (m), 943(s), 889(vs), 821(vs), 780(vs), 705(s), 534(m) (Fig. S1).

$[Cu(dap)_2(H_2O)]_2\{Cu(dap)_2[\alpha\text{-}H_2SiW_{11}O_{39}Er(H_2O)_3]_2\}\cdot 9H_2O$ (9). The synthetic procedure was identical to **3**, but $ErCl_3$ (0.047 g, 0.172 mmol) was used instead of $NdCl_3$, the amount of dap and HCl were changed to (0.20 mL, 2.356 mmol) and (0.30 mL, 2 mol L^{-1}). Purple prismatic crystals were formed. Yield: *ca.* 18% (based on $Na_{10}[A\text{-}\alpha\text{-}SiW_9O_{34}]\cdot 18H_2O$). Anal. Calcd. (found%) for $C_{18}H_{98}N_{12}O_{95}Cu_3Er_2Si_2W_{22}$ (**9**): C 3.26 (3.36), H 1.49 (1.64), N 2.54 (2.60), Cu 2.88 (2.81), Er 5.05 (4.91), Si 0.85 (0.93), W 61.01 (61.15). IR (KBr pellets, cm^{-1}): 3470(vs), 3307(w), 3251(w), 3137(w), 2965(w), 2880(w), 1618(m), 1582(m), 1453(w), 1378(w), 1169(w), 1066(m), 997(m), 944(s), 889 (vs), 821(vs), 782(vs), 705(s), 534(m) (Fig. S1).

X-Ray crystallography

Intensity data for **1–9** were collected on a Bruker APEX-II CCD diffractometer using graphite monochromatized Mo-Kα radiation (λ = 0.71073 Å) at 296(2) K. Direct methods were used to solve their structures and locate the heavy atoms using the

SHELXTL–97 program package.[10] The remaining atoms were found from successive full-matrix least-squares refinements on F^2 and Fourier syntheses. Routine Lorentz polarization and empirical absorption corrections were applied. No hydrogen atoms associated with water molecules were located from the difference Fourier map. The positions of the hydrogen atoms attached to the carbon and nitrogen atoms were geometrically placed. All hydrogen atoms were refined isotropically as a riding mode using the default SHELXTL parameters. All non-hydrogen atoms were refined anisotropically except for some oxygen atoms, carbon atoms, nitrogen atoms and water molecules (details are seen in the ESI†). The crystal data and structure refinements for **1–9** were summarized in Table 1. CCDC reference no. 876154–876162 for **1–9**, respectively. These data can be obtained free of charge from the Cambridge Crystallographic Data Centre *via* www.ccdc.cam.ac.uk/data_request/cif.

Results and discussion

Syntheses

Although some novel PTLHDs with interesting structures and fascinating properties have been reported in the past several years,[5] investigations of organic–inorganic hybrid PTLHDs have been less developed,[5b,d,g,i,m–q] especially for organic–inorganic hybrid silicotungstate-based TM–Ln heterometallic derivatives (Table 2),[5g,o,q] which offers a good chance to exploit the branch with the aim of discovering unique hybrid PTLHDs. Through a

Table 1 Crystallographic data and structural refinements for **1–9**

	1	**2**	**3**	**4**
Formula	$C_{18}H_{98}N_{12}O_{95}Cu_3Ce_2Si_2W_{22}$	$C_{18}H_{100}N_{12}O_{96}Cu_3Pr_2Si_2W_{22}$	$C_{18}H_{100}N_{12}O_{96}Cu_3Nd_2Si_2W_{22}$	$C_{18}H_{100}N_{12}O_{96}Cu_3Sm_2Si_2W_{22}$
M_r/g mol^{-1}	6574.82	6594.42	6601.08	6613.30
T/K	296(2)	296(2)	296(2)	296(2)
Crystal system	Triclinic	Triclinic	Triclinic	Triclinic
Space group	$P\bar{1}$	$P\bar{1}$	$P\bar{1}$	$P\bar{1}$
a/Å	11.519(2)	11.4614(19)	11.440(6)	11.439(3)
b/Å	12.573(2)	12.537(2)	12.590(7)	12.594(4)
c/Å	21.345(4)	21.337(3)	21.230(12)	21.357(6)
α (°)	85.877(3)	86.035(3)	85.652(11)	85.723(6)
β (°)	76.069(4)	76.034(3)	76.025(10)	75.892(6)
γ (°)	74.179(4)	74.011(3)	73.800(11)	73.965(7)
V/Å^3	2886.7(9)	2860.2(8)	2849(3)	2867.6(15)
Z	1	1	1	1
D_c/g cm^{-3}	3.782	3.829	3.847	3.830
μ/mm^{-1}	23.250	23.522	23.668	23.636
Measured reflections	14 603	14 382	13 874	14 408
Independent reflections	10 038	9939	9664	9959
R_{int}	0.0540	0.0529	0.0962	0.0593
limiting indices	$-12 \leqslant h \leqslant 13$	$-13 \leqslant h \leqslant 13$	$-10 \leqslant h \leqslant 13$	$-12 \leqslant h \leqslant 13$
	$-14 \leqslant k \leqslant 14$	$-10 \leqslant k \leqslant 14$	$-14 \leqslant k \leqslant 14$	$-14 \leqslant k \leqslant 14$
	$-25 \leqslant l \leqslant 25$	$-24 \leqslant l \leqslant 25$	$-25 \leqslant l \leqslant 25$	$-25 \leqslant l \leqslant 20$
GOF on F^2	1.022	1.020	1.065	1.054
R_1[a], wR_2[b] [$I > 2\sigma(I)$]	0.0578, 0.1473	0.0603, 0.1430	0.1103, 0.2068	0.0710, 0.1493
R_1[a], wR_2[b] [all data]	0.0783, 0.1572	0.0882, 0.1516	0.1770, 0.2197	0.1298, 0.1627
5	**6**	**7**	**8**	**9**
$C_{18}H_{100}N_{12}O_{96}Cu_3Eu_2Si_2W_{22}$	$C_{18}H_{98}N_{12}O_{95}Cu_3Gd_2Si_2W_{22}$	$C_{18}H_{96}N_{12}O_{94}Cu_3Si_2Tb_2W_{22}$	$C_{18}H_{96}Cu_3Dy_2N_{12}O_{94}Si_2W_{22}$	$C_{18}H_{98}N_{12}O_{95}Cu_3Er_2Si_2W_{22}$
6616.52	6609.08	6594.41	6601.57	6629.10
296(2)	296(2)	296(2)	296(2)	296(2)
Triclinic	Triclinic	Triclinic	Triclinic	Triclinic
$P\bar{1}$	$P\bar{1}$	$P\bar{1}$	$P\bar{1}$	$P\bar{1}$
11.3868(11)	11.383(5)	11.3793(10)	11.363(6)	11.330(2)
12.5373(12)	12.571(6)	12.5601(11)	12.518(5)	12.531(2)
21.279(2)	21.312(10)	21.3419(18)	21.355(4)	21.364(4)
85.419(2)	85.704(8)	85.533(2)	85.392(6)	85.211(3)
75.718(2)	75.841(9)	75.628(2)	75.320(3)	75.145(3)
74.056(2)	73.988(9)	74.182(2)	74.299(3)	74.548(3)
2830.4(5)	2842(2)	2842.8(4)	2829(2)	2825.4(9)
1	1	1	1	1
3.882	3.861	3.852	3.876	3.896
24.018	23.979	24.051	24.243	24.434
13 757	14 024	14 057	14 148	14 018
9647	9687	9769	9786	9726
0.0464	0.0686	0.0389	0.0851	0.0965
$-13 \leqslant h \leqslant 11$	$-13 \leqslant h \leqslant 13$	$-9 \leqslant h \leqslant 13$	$-13 \leqslant h \leqslant 8$	$-13 \leqslant h \leqslant 13$
$-14 \leqslant k \leqslant 14$	$-14 \leqslant k \leqslant 14$	$-14 \leqslant k \leqslant 14$	$-14 \leqslant k \leqslant 14$	$-14 \leqslant k \leqslant 14$
$-25 \leqslant l \leqslant 22$	$-21 \leqslant l \leqslant 25$	$-23 \leqslant l \leqslant 25$	$-25 \leqslant l \leqslant 20$	$-19 \leqslant l \leqslant 25$
1.045	1.021	1.076	1.031	1.041
0.0709, 0.1464	0.0784, 0.1686	0.0621, 0.1524	0.1045, 0.2307	0.0876, 0.1728
0.1062, 0.1566	0.1150, 0.1795	0.0825, 0.1581	0.1421, 0.2432	0.1197, 0.1810

[a] $R_1 = \sum||F_o| - |F_c||/\sum|F_o|$. [b] $wR_2 = [\sum w(F_o^2 - F_c^2)^2/\sum w(F_o^2)^2]^{1/2}$; $w = 1/[\sigma^2(F_o^2) + (xP)^2 + yP]$, $P = (F_o^2 + 2F_c^2)/3$, where $x = 0.0473$, $y = 0$ for **1**, $x = 0.0547$, $y = 0$ for **2**, $x = 0.0514$, $y = 0$ for **3**, $x = 0.0456$, $y = 0$ for **4**, $x = 0.0520$, $y = 0$ for **5**, $x = 0.0329$, $y = 0$ for **6**, $x = 0.0796$, $y = 0$ for **7**, $x = 0.1032$, $y = 0$ for **8**, $x = 0.0609$, $y = 0$ for **9**.

Table 2 Summary of the synthetic conditions of the reported silicotungstate-based TM–Ln heterometallic derivatives

Main reactants	T/°C	Synthetic method	Reaction system	Products
$K_{10}[A\text{-}\alpha\text{-}SiW_9O_{34}]\cdot 25H_2O$, $Cu(CH_3COO)_2$, $Gd(NO_3)_3/Eu(NO_3)_3/La(NO_3)_3$, ethylenediamine, HCl	140	Hydrothermal technique	H_2O	$\{[Cu(en)_2(H_2O)][(Cu(en)(OH))_3Ln(SiW_{11}O_{39})(H_2O)]\}_2\cdot 20H_2O$ ($Ln = Gd^{III}$, Eu^{II}, La^{III})[5g]
$K_{10}[A\text{-}\alpha\text{-}SiW_9O_{34}]\cdot 25H_2O$, $Cu(CH_3COO)_2$, $Gd(NO_3)_3$, ethylenediamine	140	Hydrothermal technique	NaOAc/HOAc	$[Cu(en)_2(H_2O)]_2[(GdSiW_{11}O_{39}(CH_3COO)(H_2O))_2(Cu(en)_2(H_2O))_4]\cdot 10H_2O$[5g]
$Cs_{10}[(\gamma\text{-}SiW_{10}O_{36})_2$ $(Cr(OH)(H_2O))_3]\cdot 17H_2O$, $LaCl_3\cdot 7H_2O$	80	solvent evaporation	H_2O	$[(\gamma\text{-}SiW_{10}O_{36})_2(Cr(OH)(H_2O))_3(La(H_2O)_7)_2]^{4-}$[5h]
$K_4Na_6Mn[Mn_4Si_2W_{18}O_{68}(H_2O)_2]\cdot 33H_2O$, $Ce(SO_4)_2\cdot 4H_2O$, potassium citrate	boiling	solvent evaporation	H_2O	$[\{Ce(H_2O)_7\}_2Mn_4Si_2W_{18}O_{68}(H_2O)_2]^{6-}$[5c]
$K_8[\beta_2\text{-}SiW_{11}O_{39}]\cdot 14H_2O$, Dy_2O_3/Tb_4O_7, $FeCl_3$, K_2CO_3, NaCl	160	Hydrothermal technique	H_2O	$[K_9Dy_6Fe_6(H_2O)_{12}(SiW_{10}O_{38})_6]^{26-}$ ($Ln = Dy^{III}$, Tb^{III})[5f]
$K_4[\alpha\text{-}SiW_{12}O_{40}]\cdot 17H_2O$, $GdCl_3\cdot 6H_2O/TbCl_3\cdot 6H_2O/DyCl_3\cdot 6H_2O/ErCl_3\cdot 6H_2O/LuCl_3\cdot 6H_2O$, $CuCl_2\cdot 2H_2O$, ethylenediamine (en)	170	Hydrothermal technique	H_2O	$\{[Cu(en)_2]_{1.5}Ln[(\alpha\text{-}SiW_{11}O_{39})_2]\}_2^{20-}$ ($Ln = Gd^{III}$, Tb^{III}, Dy^{III}, Er^{III}, Lu^{III})[5o]
$K_4[\alpha\text{-}SiW_{12}O_{40}]\cdot 17H_2O$, $LaCl_3\cdot 6H_2O/CeCl_3\cdot 6H_2O$, $CuCl_2\cdot 2H_2O$, ethylenediamine	170	Hydrothermal technique	H_2O	$\{[Cu(en)_2]_{1.5}Ln[(\alpha\text{-}SiW_{11}O_{39})]\}^{2-}$ ($Ln = La^{III}$, Ce^{III})[5o]
$K_4[\alpha\text{-}SiW_{12}O_{40}]\cdot 17H_2O$, $PrCl_3\cdot 6H_2O$, $CuCl_2\cdot 2H_2O$, en	170	Hydrothermal technique	H_2O	$\{[Cu(en)_2(H_2O)][Cu(en)_2]_2Pr[(\alpha\text{-}SiW_{11}O_{39})_2]\}^{7-}$[5o]
$K_4[\alpha\text{-}SiW_{12}O_{40}]\cdot 17H_2O$, $YCl_3\cdot 6H_2O/DyCl_3\cdot 6H_2O/YbCl_3\cdot 6H_2O/LuCl_3\cdot 6H_2O$, $CuCl_2\cdot 2H_2O$, pyrazine-2,3-di-carboxylate, en	170	Hydrothermal technique	H_2O	$[Cu(en)_2(H_2O)]_2\{[Cu(en)_2][Cu(en)_2(H_2O)][(\alpha\text{-}SiW_{11}O_{39})Ln(H_2O)(pzda)]\}_2^{2-}$ ($Ln = Y^{III}$, Dy^{III}, Yb^{III}, Lu^{III})[5q]
$K_8[\gamma\text{-}SiW_{10}O_{36}]\cdot 12H_2O$, $CuCl_2\cdot 2H_2O$, $Nd(NO_3)_3$, NaOH, $AlCl_3$	room temperature	solvent evaporation	H_2O	$\{Nd_2(H_2O)_{12}Cu_4(H_2O)_2(SiW_9O_{34})_2\}^{6-11}$
$Na_{10}[A\text{-}\alpha\text{-}SiW_9O_{34}]\cdot 18H_2O$, $CuCl_2\cdot 2H_2O$, $Ce(NO_3)_3\cdot 6H_2O/PrCl_3/NdCl_3/SmCl_3/EuCl_3/GdCl_3/TbCl_3/DyCl_3/ErCl_3$, dap, HCl	160	Hydrothermal technique	H_2O	**1–9**

large number of experiments, we find that it is quite difficult to design a rational synthetic route for synthesizing organic–inorganic hybrid PTLHDs using the conventional aqueous solution method at atmospheric pressure, mainly due to the fact that organic components have always very poor solubility in aqueous solution. Moreover, the competitive reactions between TM and Ln cations with POMs and organic components usually lead to immediate precipitation rather than crystallization.[4,5m,p] Thus, the conventional aqueous solution method is not suitable to explore this system. Althernatively, the hydrothermal technique is utilized. On the other hand, most of the reported organic–inorganic hybrid silicotungstate-based TM–Ln heterometallic derivatives were synthesized by means of the plenary Keggin-type silicotungstate precursors,[5o,q] however, the trivacant $[A\text{-}\alpha\text{-}SiW_9O_{34}]^{10-}$ precursor was less used and only Mialane's group reported three cubane-$\{LnCu_3(OH)_3O\}$ ($Ln = La^{III}$, Gd^{III}, Eu^{III}) inserted PTLHDs.[5g] Therefore, we recently launched a study on the reactions of trivacant Keggin-type precursors with copper and Ln cations in the presence of organoamine components under hydrothermal conditions. When the trivacant Keggin-type $[A\text{-}\alpha\text{-}PW_9O_{34}]^{9-}$ precursor was chosen, several organic–inorganic hybrid PTLHDs $[Cu(en)_2]_2H_6[Ce(\alpha\text{-}PW_{11}O_{39})_2]\cdot 8H_2O$,[12a] $[Cu(dap)_2(H_2O)][Cu(dap)_2]_{4.5}[Dy(\alpha\text{-}PW_{11}O_{39})_2]\cdot 4H_2O$,[12a] $[Cu(dap)(H_2O)_2]_{0.5}[Cu(dap)_2]_4H_2[Pr(\alpha\text{-}PW_{11}O_{39})_2]\cdot 3H_2O$,[12b] $[Cu(en)_2(H_2O)]_2[Cu(en)_2]_{1.5}H_4[Pr(\alpha\text{-}PW_{11}O_{39})_2]\cdot 10H_2O$,[12b] and $[Cu(dap)_2]_{5.5}[Y(\alpha\text{-}PW_{11}O_{39})_2]\cdot 4H_2O$[12c] have been isolated. The employment of the trivacant Keggin-type $[A\text{-}\alpha\text{-}AsW_9O_{34}]^{9-}$ precursor has led to four types of organic–inorganic hybrid PTLHDs $Na[Cu(en)_2(H_2O)]_4[Cu(en)_2]_2[Cu(H_2O)_4]_{0.5}\{Cu(en)_2[H_2Ce^{IV}(\alpha\text{-}AsW_{11}O_{39})_2]_2\}\cdot 10H_2O$, $Na_3[Cu(en)_2(H_2O)][Cu(en)_2]_{1.5}[H_3Ln(\alpha\text{-}AsW_{11}O_{39})_2]\cdot xH_2O$ ($Ln = Pr^{III}$, $x = 5$; $Ln = Nd^{III}$, $x = 4.5$; $Ln = Sm^{III}$, $x = 5.5$; $Ln = Eu^{III}$, $x = 4$; $Ln = Tb^{III}$, $x = 4$), $[Cu(dap)(H_2O)_2]_{0.5}[Cu(dap)_2(H_2O)]_2[Cu(dap)_2]_3[Ln(\alpha\text{-}AsW_{11}O_{39})_2]\cdot x\,H_2O$ ($Ln = Pr^{III}$, $x = 3$; $Ln = Eu^{III}$, $x = 3$) and $[Cu(dap)_2]_{5.5}[Ln(\alpha\text{-}AsW_{11}O_{39})_2]\cdot xH_2O$ ($Ln = Tb^{III}$, $x = 6$; $Ln = Dy^{III}$, $x = 5$).[5p] As we know, the trivacant Keggin $[A\text{-}\alpha\text{-}SiW_9O_{34}]^{10-}$ precursor has been proven to be a versatile inorganic polydentate ligand for TM cations to construct novel TM substituted silicotungstates with diverse metal nuclearities and structural topologies.[2c,8a,13] When the $[A\text{-}\alpha\text{-}SiW_9O_{34}]^{10-}$ precursor was introduced to the Cu–Ln heterometallic reaction system, a class of novel 1-D double-chain organic–inorganic hybrid silicotungstate-based Cu–Ln heterometallic derivatives **1–9** have been successfully obtained, whose structures are completely distinct from those species derived from phosphotungstates and arsenotungstates.[5p,12] As far as we know, **1–9** represent the first organic–inorganic hybrid 1-D double-chain Cu–Ln heterometallic POMs. Oddly, under similar conditions, when en replaced dap, no analogues are afforded, however, another 2-D organic–inorganic hybrid monocopper^{II}-substituted Keggin silicotungstate $[Cu(en)_2(H_2O)]_2[Cu(en)_2]_4[Si_2Cu_2W_{22}O_{78}]\cdot 7H_2O$ was always made.[14] This result indicates that dap and en have different influence on the reaction behavior of the reactants and the structural diversity of the products. Moreover, to further explore the influence of other TM ions on the structural architectures in the present system, we are using Cr^{III}, Mn^{II}, Fe^{II}, Co^{II}, Ni^{II}, Zn^{II} or Cd^{II} cations in place of the Cu^{II} ion to perform the related exploitation. In addition, although the $[A\text{-}\alpha\text{-}SiW_9O_{34}]^{10-}$ starting material was employed to prepare **1–9**, all the products include the $[\alpha\text{-}SiW_{11}O_{39}]^{8-}$ fragments. However, when $K_8[\alpha\text{-}SiW_{11}O_{39}]\cdot 13H_2O$ replaced Na_{10} $[A\text{-}\alpha\text{-}SiW_9O_{34}]\cdot 18H_2O$ under similar conditions, **1–9** could not be afforded, which suggests that the transformation of $[A\text{-}\alpha\text{-}SiW_9O_{34}]^{10-} \rightarrow [\alpha\text{-}SiW_{11}O_{39}]^{8-}$ plays an important role in the formation of **1–9**. This transformation has already been observed in previous studies.[5g]

Structural descriptions

Single-crystal X-ray diffraction analyses show that **1–9** are isomorphic only with slight differences in bond length, bond angle and the number of lattice waters. They all exhibit the novel 1-D double-chain formed by dimeric Cu–Ln heterometallic silicotungstate units $[Cu(dap)_2(H_2O)]_2\{Cu(dap)_2[\alpha\text{-}H_2SiW_{11}O_{39}Ln(H_2O)_3]_2\}$ [Ln = Ce^{III} (**1**), Pr^{III} (**2**), Nd^{III} (**3**), Sm^{III} (**4**), Eu^{III} (**5**), Gd^{III} (**6**), Tb^{III} (**7**), Dy^{III} (**8**), Er^{III} (**9**)] by means of the bridging role of the Ln cations, as a result, only the structure of **1** is described in details. Due to the existence of the octahedral geometries of the Cu^{II} ions in **1–9**, the evident Jahn–Teller effect occurs and leads to elongation of the Cu–O distances in the crystal field,[15] therefore the Cu–O weak interactions will be considered in the structural descriptions.

Compound **1** crystallizes in the triclinic space group $P\bar{1}$ and its asymmetrical molecular structural unit (Fig. 1a) consists of 1 mono-Ce^{III} substituted Keggin-type $[\alpha\text{-}SiW_{11}O_{39}Ce(H_2O)_3]^{5-}$ (**1a**) fragment, 0.5 bridging $[Cu(dap)_2]^{2+}$ cation, 1 supporting $[Cu(dap)_2(H_2O)]^{2+}$ cation, 2 protons and 4.5 lattice water molecules. Based on the charge balance consideration, 2 protons should be added to the asymmetrical molecular structural unit of **1**. In order to localize possible binding sites of 2 protons, bond valence sum (BVS) calculations have also been performed on all oxygen atoms of the POM framework (Table S1†).[16] The results show that the BVS values (1.60, 1.52) of O23 and O38 are significantly lower than 2, indicating that two oxygen atoms may be monoprotonated. Therefore, the asymmetrical molecular structural unit of **1** is formulated as $[Cu(dap)_2(H_2O)]\{Cu(dap)[\alpha\text{-}H_2SiW_{11}O_{39}Ce(H_2O)_3]\}\cdot 4.5H_2O$. As a matter of fact, such phenomena where protons are located on the POM framework by means of BVS calculations are often encountered in previous studies.[5g,h,8a] In the asymmetrical molecular structural unit, the pendant $[Cu1(dap)_2(H_2O)]^{2+}$ cation links to **1a** *via* a terminal oxygen atom and is embedded in a severely distorted octahedral geometry, in which four nitrogen atoms from two dap ligands occupy the basal plane [Cu–N: 2.012(19)–2.05(2) Å] and a terminal oxygen atom [Cu–O: 3.309(15) Å] and a water oxygen atom [Cu–O: 2.259(15) Å] stand on the axial positions. The bridging $[Cu2(dap)_2]^{2+}$ cation is located on the special site leading to an occupancy of 50% and inhibits the elongated octahedron defined by four nitrogen atoms from two dap ligands with Cu–N distances of 2.033(6)–2.110(6) Å building the equatorial plane and two oxygen atoms from two adjacent **1a** fragments with long Cu–O distances of 3.322(17) Å occupying two polar sites. As shown above, the $[Cu1(dap)_2(H_2O)]^{2+}$ and $[Cu2(dap)_2]^{2+}$ cations display elongated octahedral geometries, indicating that Cu1 and Cu2 cations adopt an electron configuration of $(t_{2g})^6(d_{x2\text{-}y2})^2(d_{z2})^1$. The $Ce1^{3+}$ cation incorporated into the vacant site of the $[\alpha\text{-}SiW_{11}O_{39}]^{8-}$ subunit exhibits an eight-coordinate distorted square antiprism geometry (Fig. 1b), in which three coordinate oxygen atoms come from three water ligands [Ce–O: 2.50(2)–2.628(17) Å], four from one $[\alpha\text{-}SiW_{11}O_{39}]^{8-}$ subunit [Ce–O: 2.403(13)–2.433(12) Å] and one from the other $[\alpha\text{-}SiW_{11}O_{39}]^{8-}$ subunit on the neighbouring **1a** fragment [Ce–O: 2.498(13) Å]. The Ce–O distances are within the usual range and consistent with those described in the literature.[5i,17] In the coordinate polyhedron around the $Ce1^{3+}$ cation, the O11, O1W, O2W and O3W group and the O20, O24, O36 and O39 group constitute two bottom planes of the square antiprism and the average deviations from their ideal planes are 0.0862 and 0.0147 Å, respectively. The distances between the $Ce1^{3+}$ cation and the two bottom planes are 1.4451 and 1.1833 Å, respectively. The Ce1–O11A [A: –1 + *x*, *y*, *z*] distance [2.498(13) Å] is much longer than those of other Ce–O [Ce1–O20, Ce1–O24, Ce1–O36, Ce1–O29] distances because the W–O–Ce1–O11A–W linkage acts as the bridge forming the 1-D chain structure. Notably, the mono-Ce^{III} substituted Keggin-type **1a** is the hardcore component of **1**. Actually, the mono-Ln substituted Keggin-type silicotungstates have more than 40 years of history since Peacock and Weakley first put forward in 1971 the claim that a combination of monovacant Keggin polyoxoanions $[SiW_{11}O_{39}]^{8-}$ with Ln cations can form both 1 : 1–type and 1 : 2–type derivatives in solution.[18] In 2000, Pope *et al.* employed a simple strategy to isolate and characterize first two infinite 1-D 1 : 1–type POM-based Ln derivatives $[Ln(\alpha\text{-}SiW_{11}O_{39})(H_2O)_3]^{5-}$ (Ln = La^{III}, Ce^{III}), which represent two types of polymeric chain structures in the solid state.[19] In 2003, Mialane *et al.* also reported the solid-state structures of the Ln/$[\alpha\text{-}SiW_{11}O_{39}]^{8-}$ (Ln = Yb^{III}, Nd^{III}, Eu^{III}, Gd^{III}).[20] In 2004, Mialane *et al.* found the dimeric $[(SiW_{11}O_{39}Ln)_2(\mu\text{-}CH_3COO)_2]^{12-}$ (Ln = Gd^{III}, Yb^{III}) complexes.[21] In 2006, we addressed two 1-D and 2-D organic–inorganic hybrid mono-Sm^{III} substituted Keggin-type silicotungstates $\{Sm(H_2O)_7[Sm(H_2O)_2(DMSO)(\alpha\text{-}SiW_{11}O_{39})]\}^{2-}$ and $\{[Sm(H_2O)_{5.5}(DMF)_{0.5}]_2[Sm(H_2O)_2(DMF)][Sm(H_2O)_3(\alpha\text{-}SiW_{11}O_{39})]_2\}^{-}$.[22] Different from those previously reported mono-Ln^{III}

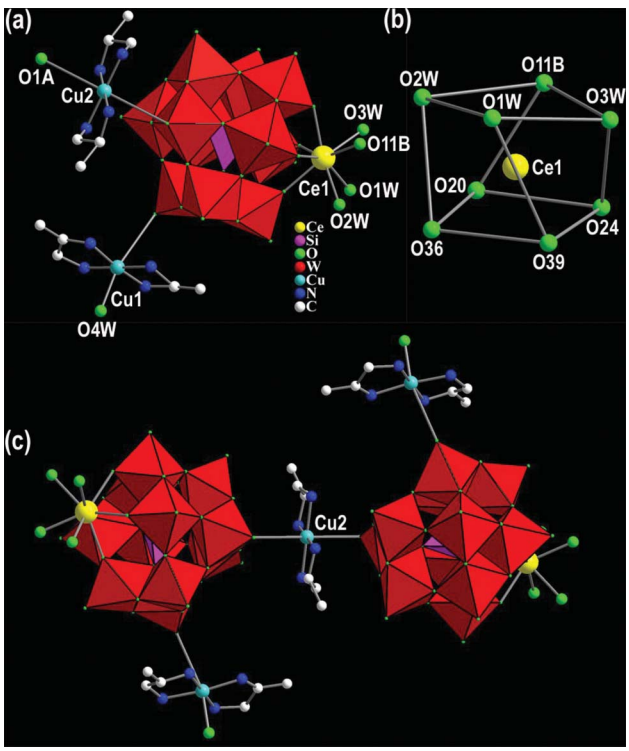

Fig. 1 a) The asymmetrical molecular structural unit of **1** with selected numbering scheme. b) The eight-coordinate distorted square antiprism geometry of the Ce1 cation. c) The dimeric molecular structural fragment $[Cu(dap)_2(H_2O)]_2H_4\{Cu(dap)_2[\alpha\text{-}SiW_{11}O_{39}Ce(H_2O)_3]_2\}$ of **1**. The atoms with "A, B" in their labels are symmetrically generated (A: 4 − *x*, 2 − *y*, −*z*; B: −1 + *x*, *y*, *z*). Hydrogen atoms, protons and lattice water molecules are omitted for clarity.

substituted Keggin-type silicotungstate molecular structural units,[18–22] the molecular structural fragment $[Cu(dap)_2(H_2O)]_2\{Cu(dap)_2[\alpha\text{-}H_2SiW_{11}O_{39}Ce(H_2O)_3]_2\}$ of **1** contains the Cu^{II}–Ce[III] heterometallic cations and can be viewed as a fusion of two asymmetrical units $[Cu(dap)_2(H_2O)]\{Cu(dap)[\alpha\text{-}H_2SiW_{11}O_{39}Ce(H_2O)_3]\}$ by the connection of the bridging $[Cu2(dap)_2]^{2+}$ cation (Fig. 1c). For all we know, such 2 : 2–type Cu^{II}–Ln^{III} heterometallic dimeric molecular structural fragment (2 : 2 is the molar ratio of $Ln/SiW_{11}O_{39}$) is firstly observed in POM chemistry although some 2 : 1–type Cu^{III}–Ln^{III} heterometallic molecular structural fragments $\{[Cu(en)_2]_{1.5}Ln[(\alpha\text{-}SiW_{11}O_{39})_2]\}_2^{20-}$ (Ln = Gd^{III}, Tb^{III}, Dy^{III}, Er^{III}, Lu^{III})[5o] and 2 : 2–type Ln^{III}-containing dimeric molecular structural fragments $[(\alpha\text{-}SiW_{11}O_{39}Ln)_2(\mu\text{-}CH_3COO)_2]^{12-}$ (Ln = Gd^{III}, Yb^{III})[21] have already been communicated.

The most striking structural feature of **1** is that each $[Cu(dap)_2(H_2O)]_2\{Cu(dap)_2[\alpha\text{-}H_2SiW_{11}O_{39}Ce(H_2O)_3]_2\}$ links two adjacent identical units through four W–O–Ce1–O11–W bridges and construct the beautiful 1-D double-chain structure (Fig. 2a). To our knowledge, **1** still represents the first organic–inorganic hybrid 1-D double-chain PTLHD although an organic–inorganic hybrid germanotungstate-based Sm^{III}-containing 1-D double-chain $[Sm_2(\alpha\text{-}GeW_{11}O_{39})(DMSO)_3(H_2O)_6]^{2-}$ (Fig. 2b)[22] and an inorganic silicotungstate-based Cr^{III}–La^{III} heterometallic 1-D double-chain $[(\gamma\text{-}SiW_{10}O_{36})_2(Cr(OH)(H_2O))_3(La(H_2O)_7)_2]^{4-}$ (Fig. 2c)[5h] have been reported by Niu and Mialane, respectively. Comparing **1** with $[Sm_2(\alpha\text{-}GeW_{11}O_{39})(DMSO)_3(H_2O)_6]^{2-}$,[22] four obvious discrepancies are observed albeit some similarities exist: (a) the former was synthesized by the trivacant $[A\text{-}\alpha\text{-}SiW_9O_{34}]^{10-}$ precursor under hydrothermal conditions, on the contrary, the latter was prepared by the monovacant $[\alpha\text{-}GeW_{11}O_{39}]^{8-}$ precursor in the conventional aqueous solution; (b) the former is an organic–inorganic hybrid POM-based TM–Ln heterometallic 1-D double-chain while the latter is an organic–inorganic hybrid POM-based Ln-containing 1-D double-chain; (c) the 1-D double chains in the former are connected by $[Cu(en)_2]^{2+}$ bridges whereas the 1-D double chains in the latter are linked by $[Sm(DMSO)_2(H_2O)_2]^{3+}$ linkers; (d) the dap ligands chelate the copper ions in the former, however, the DMSO ligands coordinate to the samarium ions in the latter. In comparison with **1**, three evident differences are seen in $[(\gamma\text{-}SiW_{10}O_{36})_2(Cr(OH)(H_2O))_3(La(H_2O)_7)_2]^{4-}$:[5h] (a) it was made by the preformed $Cs_{10}[(\gamma\text{-}SiW_{10}O_{36})_2(Cr(OH)(H_2O))_3]\cdot 17H_2O$ precursor in the conventional aqueous solution; (b) it is an inorganic POM-based TM–Ln heterometallic 1-D double-chain; (c) its 1-D double chains are bridged by $[La(H_2O)_7]^{3+}$ cations. Apparently, the occurrence of these distinguishing 1-D double-chain motifs manifests the structural diversity of POM chemistry.

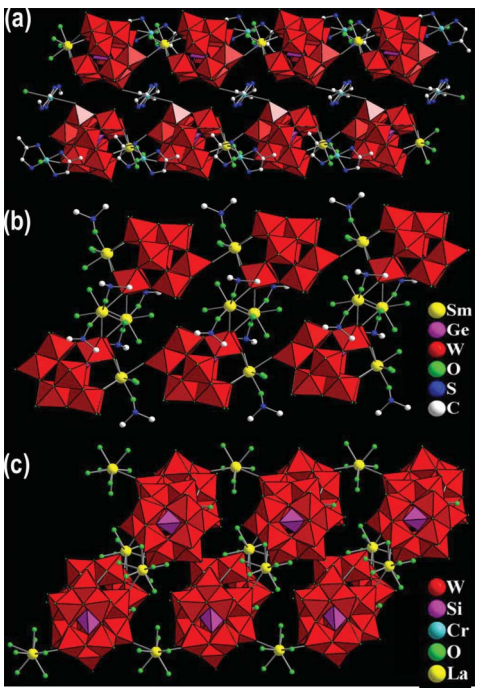

Fig. 2 a) The organic–inorganic hybrid silicotungstate-based Cu^{II}–Ce^{III} heterometallic 1-D double-chain architecture of **1**. b) The organic–inorganic hybrid germanotungstate-based Sm^{III}-containing 1-D double-chain structure of $[Sm_2(\alpha\text{-}GeW_{11}O_{39})(DMSO)_3(H_2O)_6]^{2-}$.[22] c) The inorganic silicotungstate-based Cr^{III}–La^{III} heterometallic 1-D double-chain structure of $[(\gamma\text{-}SiW_{10}O_{36})_2(Cr(OH)(H_2O))_3(La(H_2O)_7)_2]^{4-}$.[5h]

Intriguingly, the 1-D double-chains in **1** are aligned in the arrangement mode of –AAA– along the crystallographical *b* and *c* axes (Fig. 3). In addition, from the viewpoint of supramelocular chemistry, Keggin-based supramolecular architectures are looked on as one of the most promising potentially applied materials in the field of chemistry, biology and material sciences.[23] Actually, supramolecular architectures are also present in **1–9** in view of hydrogen-bonding interactions between nitrogen atoms of dap ligands and surface oxygen atoms of POM fragments or water molecules. Specifically, dap ligands on copper cations work as the proton donors, surface oxygen atoms of mono-Ln substituted Keggin silicotungstates and water molecules function as the proton acceptors, and then donors and acceptors are hydrogen-bonded together creating the 3-D extended supramolecular architectures. The N–H···O distances are in the range of 2.93(2)–3.467(19) Å for **1**, 3.00(3)–3.67(2) Å for **2**, 3.02(6)–3.42(6) Å for **3**, 3.00(2)–3.34(4) Å for **4**, 2.8388(3)–3.3076(4) Å for **5**, 2.99(4)–3.36(3) Å for **6**, 2.97(2)–3.45(4) Å for **7**, 2.99(3)–3.34(3) Å for **8**, and 2.99(4)–3.29(5) Å for **9**.

IR and UV-Vis spectra

IR spectra of **1–9** have been recorded between 4000 and 400 cm^{-1} with KBr pellets (Fig. S1).† In the low-wavenumber region, IR spectra of **1–9** display the characteristic vibration patterns derived from the Keggin-type POM framework and are somewhat similar

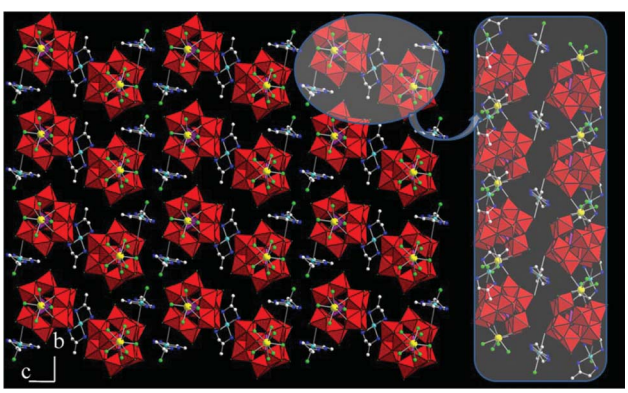

Fig. 3 Arrangement of 1-D double-chains in the crystallographical *bc* plane in **1**, showing the mode of –AAA–.

to that of the monovacant Keggin-type $K_8[\alpha\text{-}SiW_{11}O_{39}]\cdot 13H_2O$ (Fig. S2), because they all consist of the C_s-symmetrical $[\alpha\text{-}SiW_{11}O_{39}]^{8-}$ fragments. In contrast, IR spectra of **1–9** obviously differ from that of $Na_{10}[A\text{-}\alpha\text{-}SiW_9O_{34}]\cdot 18H_2O$ (Fig. S3), which further confirms the structural transformation of $[A\text{-}\alpha\text{-}SiW_9O_{34}]^{10-} \rightarrow [\alpha\text{-}SiW_{11}O_{39}]^{8-}$ during the course of forming **1–9**. In general, the feature bands can be easily assigned in comparison with the corresponding bands of the monovacant or plenary Keggin clusters. Four strong characteristic vibration bands in IR spectra of **1–9** corresponging to the terminal $\nu_{as}(W\text{–}O_t)$, $\nu_{as}(Si\text{–}O_a)$, corner-sharing $\nu_{as}(W\text{–}O_b)$ and edge-sharing $\nu_{as}(W\text{–}O_c)$ stretching vibration appear at 948–943; 889–883; 828–820, 782–775; and 705–699 cm^{-1}, respectively. Comparing with $K_8[\alpha\text{-}SiW_{11}O_{39}]\cdot 13H_2O$, the $\nu_{as}(W\text{–}O_t)$ vibration bands for **1–9** have different red-shifts of 14–19 cm^{-1}, the possible major reason for which may be that Ln^{III} cations, $[Cu(dap)_2(H_2O)]^{2+}$ and $[Cu(dap)_2]^{2+}$ cations have strong interactions to the terminal oxygen atoms of the $[\alpha\text{-}SiW_{11}O_{39}]^{8-}$ fragments, impairing the W–O_t bonds, reducing the W–O_t bond force constant and leading to decreasing of the W–O_t vibration frequency.[22] In comparison with $K_4[\alpha\text{-}SiW_{12}O_{40}]\cdot xH_2O$,[24] the $\nu_{as}(W\text{–}O_b)$ vibration bands for **1–9** split into two bands as a result of the fact that Ln cations incorporate into the vacant sites of the $[\alpha\text{-}SiW_{11}O_{39}]^{8-}$ fragments resulting in the lower symmetry of the monovacant $[\alpha\text{-}SiW_{11}O_{39}]^{8-}$ fragments in **1–9** than that of the plenary $[\alpha\text{-}SiW_{12}O_{40}]^{4-}$ moiety. Furthermore, the characteristic vibration bands of dap ligands are also observed in IR spectra. The signals appearing at 3307–3137 cm^{-1} and 2967–2960 cm^{-1} are attributable to the $\nu(NH_2)$ and $\nu(CH_2)$ stretching vibration while the resonances centered at 1629–1581 cm^{-1} and 1460–1453 cm^{-1} are assigned to the $\delta(NH_2)$ and $\delta(CH_2)$ bending vibration, respectively.[1j,6,8a] Additionally, the vibration bands centered at 3476–3464 cm^{-1} are indicative of the presence of lattice water molecules or coordination water molecules. In short, the results of IR spectra are in good agreement with X-ray single-crystal structural analyses. However there is no evidence of the Ln–O stretching vibration in the IR region, probably due to the predominantly ionic characteristic of the interactions between the the $[\alpha\text{-}SiW_{11}O_{39}]^{8-}$ fragments and the Ln centres.[17b,25] UV-Vis spectra of **1–9** performed in aqueous solution in the range of 190–800 nm have been recorded at room temperature (Fig. S4, S5).† UV spectra of **1–9** reveal only one broad lower energy absorption band centered at 247–255 nm (Fig. S4),† which is assigned to the pπ–dπ charge-transfer transitions of the $O_{b(c)} \rightarrow W$ bonds. However, the higher energy absorption band attributed to the pπ–dπ charge-transfer transitions of the $O_t \rightarrow W$ bonds is blue-shifted to the near UV region that is lower than 190 nm, which may be related to the coordination of Ln cations and/or Cu^{II}-dap complexes to POM matrixes. The visible spectra of **1–9** do not exhibit the absorption bands attributable to the d–d transitions of Cu^{II} cations and the f–f transitions of Ln^{III} cations (Fig. S5),† which may be in relation to the small solubility of **1–9** in water (because **1–9** were prepared under hydrothermal conditions).

Magnetic properties

Recently, heterometallic TM–Ln complexes have attracted growing interest due to the presence of exchange interactions between spin carriers in the solid-state chemistry and material science.[26] Because there exist Cu–Ln heterometal cations in **1–9**, the magnetic properties of only **2**, **3**, **6** and **8** have been investigated as examples below. Their magnetic susceptibilities have been measured in the temperature range of 2.7–300 K on a Quantum Design MPMS–5 SQUID magnetometer in an applied magnetic field of 2000 Oe (Fig. 4) and the basic magnetic data derived from these measurements are listed in Table 3. Although numerous TM–Ln complexes have been described,[27] except for the isotropic Gd^{III} cation having a $^8S_{7/2}$ single-ion ground state, not much is known about the nature and magnitude of the exchange interaction of Ln cations between themselves and with other magnetic groups and the evolution of the magnetic properties along the Ln series,[28] one reason for which is that the orbital contribution occurs for the most Ln cations and the

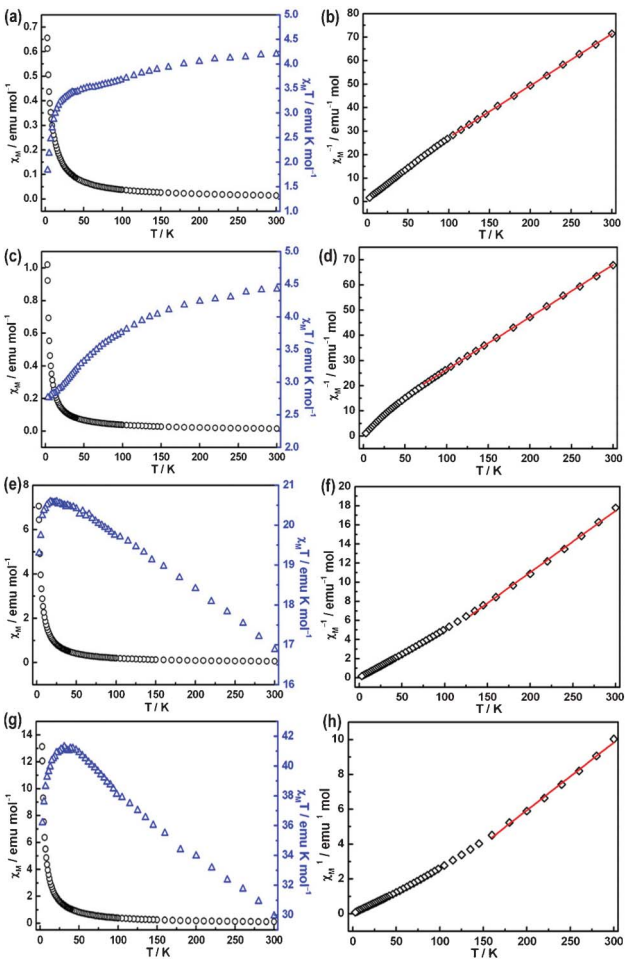

Fig. 4 (a) Temperature dependence of the magnetic susceptibility for **2**(Pr) between 2.7 and 300 K. (b) Temperature evolution of the inverse magnetic susceptibility for **2**(Pr) between 33 and 300 K. (c) Temperature dependence of the magnetic susceptibility for **3**(Nd) between 2.7 and 300 K. (d) Temperature evolution of the inverse magnetic susceptibility for **3**(Nd) between 70 and 300 K. (e) Temperature dependence of the magnetic susceptibility for **6**(Gd) between 2.7 and 300 K. (f) Temperature evolution of the inverse magnetic susceptibility for **6**(Gd) between 126 and 300 K. (g) Temperature dependence of the magnetic susceptibility for **8**(Dy) between 2.7 and 300 K. (h) Temperature evolution of the inverse magnetic susceptibility for **8**(Dy) between 159 and 300 K. The red solid line was generated from the best fit by the Curie–Weiss expression.

Table 3 Summary of static magnetic properties of **2**(Pr), **3**(Nd), **6**(Gd) and **8**(Dy)

	2	**3**	**6**	**8**
ground state of Ln	$^3H_4$	$^4I_{9/2}$	$^8S_{7/2}$	$^6H_{15/2}$
expected $\chi_M T$ at 300 K, emu K mol^{-1}	4.33	4.41	16.87	29.47
observed $\chi_M T$ at 300 K, emu K mol^{-1}	4.20	4.42	16.88	29.93
observed $\chi_M T$ at 2.7 K, emu K mol^{-1}	1.76	2.74	19.06	35.30
Curie constant C, emu K mol^{-1}	4.54	4.81	15.50	25.68
Weiss constant θ, K	−23.92	−27.00	29.06	47.59

ligand field effect on the magnetic characteristics of the ions displays the spin–orbit coupling, which makes the quantitative interpretation of the magnetic data of their complexes very complicated.[28] The $^{2S+1}$L group term of the 4f^n configuration for a Ln cation is often split into $^{2S+1}L_J$ spectroscopic levels by interelectronic repulsion and spin–orbit coupling. Each of these states is further split into Stark sublevels by the crystal field perturbation.[28,29] As a result, the orbital component contribution of the magnetic moment is more important for Ln cations than that of TM cations since crystal-field effects are smaller and spin–orbit coupling is larger for Ln cations.[30] The major difficulty in analyzing the magnetic properties of the Cu–Ln complexes lies in the case that the ground state of the Ln cations (Ln ≠ La^{III}, Gd^{III}, Lu^{III}) has a first-order angular momentum, preventing the use of the spin-only isotropic Hamiltonian.[31] At room temperature, all Stark sublevels of the $^{2S+1}L_J$ ground state or those of the low-lying first excited states for Sm^{III} and Eu^{III} cations are thermally populated. As the temperature drops, depopulation of these sublevels occurs and consequently the $\chi_{Ln}T$ decreases (χ_{Ln} is the magnetic susceptibility of the Ln cation). The temperature dependence of the χ_{Ln} deviates with respect to the Curie law.[28,31c] When the Ln cation interacts with the second paramagnetic species (such as TM cations), the temperature dependence of the $\chi_M T$ is due to both the variation of $\chi_{Ln}T$ and the coupling between the Ln cation and the other paramagnetic species. Consequently, the nature of interactions between a Ln cation with a first-order orbital momentum and the second paramagnetic species cannot be unambiguously deduced only from the shape of the $\chi_M T$ *versus* T curve or θ values.[28,32] Additionally, for most of the Ln compounds, the $\chi_M T$ value at room temperature is close to what is predicted in the free-ion approximation for the cases where only one level, $^{2S+1}L_J$, is thermally populated and second-order contributions are ignored.[33,27d] For the complexes containing the Sm^{III} and Eu^{III} ions, magnetic susceptibility is affected by the thermally populated excited states because of the small energy separation [1000 cm^{-1} for Sm^{III} and 400 cm^{-1} for Eu^{III}]. In **1–9**, the distances between copper centers and Ln centers are very long and their magnetisms mainly exhibit free-ion behavior. Therefore, the magnetic properties of **2**, **3**, **6** and **8** are preliminarily investigated as examples.

For **2**, the χ_M slowly increases from 0.01 emu mol^{-1} at 300 K to 0.10 emu mol^{-1} at 35 K, then exponentially to the maximum of 0.66 emu mol^{-1} at 2.7 K (Fig. 4a). The $\chi_M T$ value is equal to 4.20 emu K mol^{-1} at 300 K, which is close to the expected value of 4.33 emu K mol^{-1} for three noninteracting Cu^{II} ions with S = 1/2 and g = 2.00) and two isolated Pr^{III} cations ($^3H_4$, J = 4, g = 4/5)[34]. The $\chi_M T$ value declines gradually between 300 and 33 K, where the $\chi_M T$ value is 3.40 emu K mol^{-1} K. Below 33 K, it falls sharply to 1.76 emu K mol^{-1} at 2.7 K. This decline is intimately related to the depopulation of the Stark levels upon cooling. Fitting the data of $\chi_M{}^{-1}$ *versus* T between 300 and 105 K to the Curie–Weiss law gives C = 4.54 emu K mol^{-1} and θ = −23.92 K (Fig. 4b). The θ value is large, indicating the importance of ligand field effects in **2**.[32]

With respect to **3**, the value of $\chi_M T$ is 4.42 emu K mol^{-1} at 300 K, which is consistent with the expected value of 4.41 emu K mol^{-1} for three noncorrelated Cu^{II} ions with S = 1/2 and g = 2.00) and two isolated Nd^{III} cations ($^4I_{9/2}$, J = 9/2, g = 8/11), and decreases slowly to 2.74 emu K mol^{-1} at 2 K (Fig. 4c). This behavior is mainly due to the splitting of the 10-fold degenerate $^4I_{9/2}$ ground state of the Nd^{III} cations affected by the crystal field perturbation and the progressive depopulation of the higher energy state upon cooling.[29] The whole profile of $\chi_M T$ *versus* T is very similar to those previously reported mononuclear and homodinuclear Nd^{III} complexes.[29,31c,35] Actually, similar magnetic behavior has been observed in the Nd-substituted POM [{(α-PW$_{11}$O$_{39}$H)Nd(H$_2$O)$_3$}$_2$]$^{6-}$ communicated by us.[36] The relationship of $\chi_M{}^{-1}$ *versus* T in 70–300 K obeys the Curie–Weiss law, however, as the temperature decreases from 70 to 2.7 K, the relation of $\chi_M{}^{-1}$ *versus* T does not follow the Curie–Weiss law (Fig. 4d). It is well-known that the depopulation of the Nd^{III} Stark levels as temperature decreases is a distinct magnetic phenomenon. The $^4I_{9/2}$ ground state for the free Nd^{III} ion in the crystal field is split into five Kramers doublets.[31c] At room temperature, those doublets are equally populated. When temperature decreases, the Kramers doublets of higher energy are successively depopulated and the magnetic behavior deviates from the Curie–Weiss law predicated by the free-ion approximation.[37]

In the case of **6**, at room temperature, $\chi_M T$ is equal to 16.88 emu K mol^{-1}. This value corresponds to that expected for two free Gd^{III} and three Cu^{II} noninteracting magnetic centers with the local g factors g_{Gd} = g_{Cu} = 2.0. When temperature is lowered, $\chi_M T$ gradually increases the maximum of 20.59 emu K mol^{-1} at 17 K (Fig. 4e). This behavior may indicate that the S_{Gd} = 7/2 local spins somewhat tend to align along the same direction.[38] Those data, however, do not specify whether the S_{Cu} = 1/2 local spins of the Cu-dap groups align along the same direction (ferromagnetic behavior) or along the opposite direction (ferrimagnetic behavior).[38] In the 126–300 K temperature range, these magnetic susceptibility data could be described by a Curie–Weiss law with a Weiss constant θ = 29.06 K (Fig. 4f), being consistent with the dominant ferromagnetic coupling interactions. In addition, a sudden decrease of the $\chi_M T$ value below 17 K can be ascribed to the intermolecular antiferromagnetic interactions.

For **8**, the value of $\chi_M T$ at 300 K is 29.93 emu mol^{-1} K, in line with the sum (29.47 emu K mol^{-1}) of the contribution attributable to three non-interacting Cu^{II} cations (S = 1/2) with g = 2.00 and two free Dy^{III} cation in the $^6H_{15/2}$ group state (J = 15/2, g = 4/3).[39a,39b] The $\chi_M T$ increases to a maximum of 41.32 emu mol^{-1} K at 34 K upon cooling (Fig. 4g). This behavior of the $\chi_M T$ *versus* T plot may indicate that the S_{Gd} = 5/2 local spins somewhat tend to align along the same direction. Fitting the high-temperature susceptibility ($159 < T < 300$) to the Curie–Weiss law results in values of C = 25.68 emu K mol^{-1} and θ = 47.59 K (Fig. 4h), which may be indicative of the ferromagnetic coupling interactions. The decrease in $\chi_M T$ on decreasing the temperature from 34 to 2.7 K can be ascribed

to the intermolecular antiferromagnetic interactions and the thermal depopulation of Stark sublevels of the Dy^{III} cations.[39c,39d] Generally, the Dy^{III} cation with a first-order orbital momentum has the $^6H_{15/2}$ ground state, which is split into eight Stark components in the low symmetrical crystal field, each of them being a Kramers doublet. The energy gap between the highest and lowest Kramers doublets is on the order of a few hundreds of wavenumbers.[39e] Upon cooling, the highest Kramers doublets are progressively depopulated, and at 2.7 K only the ground Kramers doublet is populated. This situation often results in pronounced deviation of the magnetic behavior from the Curie law (Fig. 4h).

Photoluminescence properties

Ln-based complexes can show fascinating photoluminescent properties and technological applications in areas such as light-emitting diodes, optical fibers, lasers, optical amplifiers, NIR-emitting materials, plasma displays and sensory probes,[40] which is mainly related to the electronic properties of the Ln ions: the shielding of the 4f electrons by the outer 5s and 5p electrons results in well-defined absorption and emission bands.[41] As a consequence, Ln ions retain their atomic properties upon complex formation. Ln-containing POMs can be viewed as discrete molecular analogues of rare-earth phosphors. Photoexcitation of the O → M (M = Mo or W) ligand to metal charge transfer (LMCT) bands of the POM ligands can result in intramolecular energy transfer from the O → M excited states to excited energy levels of Ln^{III} ions, thereby sensitizing Ln^{III} emission.[42] Yamase's comprehensive studies have offered considerable insight into the molecular mechanisms of these energy transfer processes.[43] The emission characteristics of Ln^{III} ions are highly dependent on the nature of POM ligands, the symmetry and coordination geometry at the Ln centers and the number of aqua coligands. Indeed, POM ligands bound to Ln^{III} ions are often polydentate, minimizing the coligation of aqua and similar ligands, which consist of high frequency O–H and N–H oscillators that otherwise tend to quench the luminescence emission.[42] Therefore, the solid-state photoluminescence properties of **4**, **5**, **7** and **8** have been investigated at room temperature. Excitation of the as-synthesized solid of **4** at 302 nm leads to pink emission of the Sm^{III} ions due to the $^4G_{5/2} \rightarrow {}^6H_J$ (J = 5/2, 7/2 and 9/2) transitions, which appear at *ca.* 570, 603 and 635 nm, respectively. The most intense peak is the transition $^4G_{5/2} \rightarrow {}^6H_{7/2}$ at 603 nm (Fig. 5a). These are comparable to the previous results.[44] Furthermore, when the as-synthesized solid of **4** is emitted at 570 nm, an excitation profile is obtained that well matches the excitation spectrum of **4**. Sm^{III} centers in **4** have

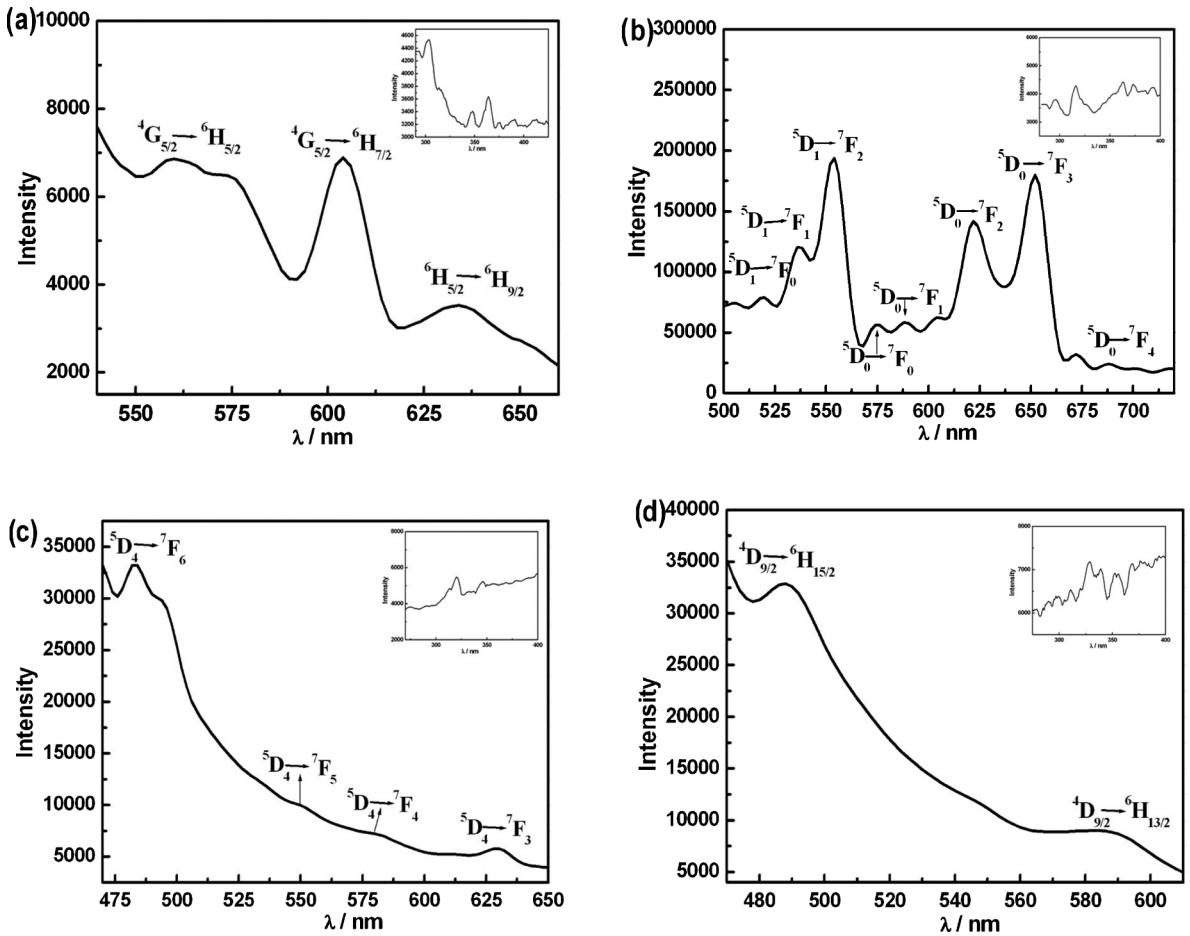

Fig. 5 Solid-state emission spectra (a), (b), (c) and (d) for **4**(Sm) (λ_{ex} = 302 nm), **5**(Eu) (λ_{ex} = 310 nm), **7**(Tb) (λ_{ex} = 320 nm) and **8**(Dy) (λ_{ex} = 310 nm) at room temperature. Inset: The solid-state excitation spectra (a), (b), (c) and (d) for **4**(Sm) (λ_{em} = 570 nm), **5**(Eu) (λ_{em} = 554 nm), **7**(Tb) (λ_{em} = 484 nm) and **8**(Dy) (λ_{em} = 488 nm) at room temperature.

three aqua ligands, which can give rise to quenching of the Sm^{III} emission and shortening the luminescence lifetimes through nonradiative relaxation processes involving OH oscillators.[45] Excitation of the as-synthesized solid of **5** at 310 nm reveals eight emission bands of the Eu^{III} ions (Fig. 5b), which are attributed to $^5D_1 \rightarrow {}^7F_J$ (J = 0, 1, 2) [$^5D_1 \rightarrow {}^7F_0$ (519 nm), $^5D_1 \rightarrow {}^7F_1$ (536 nm), $^5D_1 \rightarrow {}^7F_2$ (554 nm)] and $^5D_0 \rightarrow {}^7F_J$ (J = 0, 1, 2, 3, 4) [$^5D_0 \rightarrow {}^7F_0$ (575 nm), $^5D_0 \rightarrow {}^7F_1$ (589 nm), $^5D_0 \rightarrow {}^7F_2$ (623 nm), $^5D_0 \rightarrow {}^7F_3$ (653 nm), $^5D_0 \rightarrow {}^7F_4$ (688 nm)] transitions, respectively.[46] The $^5D_0 \rightarrow {}^7F_{1,3}$ transitions are magnetic dipole transitions and insensitive to their local environments while the $^5D_0 \rightarrow {}^7F_{0,2,4}$ transitions are electric dipole transitions and hypersensitive to their local environments.[47] The $^5D_0 \rightarrow {}^7F_0$ transition is strictly forbidden in a field of symmetry, but this symmetric forbidden transition at 575 nm can hardly be found in **5**, suggesting that **5** untilizes comparatively higher symmetry. The $^5D_0 \rightarrow {}^7F_1$ transition at 589 nm is a magnetic-dipole transition and its intensity varies with the crystal field strength acting on Eu^{III} ions. The $^5D_0 \rightarrow {}^7F_2$ transition at 623 nm is an electric dipole transition and is extremely sensitive to the chemical bonds in the vicinity of Eu^{III} ions. In a site environment with inversion symmetry, the $^5D_0 \rightarrow {}^7F_1$ magnetic dipole transition is dominant while in a site environment without inversion symmetry, the $^5D_0 \rightarrow {}^7F_2$ electronic dipole transition becomes the strongest one.[5p,48] Furthermore, the intensity of the $^5D_0 \rightarrow {}^7F_2$ transition increases as the site symmetry of Eu^{III} ions decreases. As a result, the intensity ratio of the $^5D_0 \rightarrow {}^7F_2$/the $^5D_0 \rightarrow {}^7F_1$ transition is widely used to examine the chemical microenviroment of around the Eu^{III} ions and is used as a measure of the site symmetry of the Eu^{III} ions.[49] For **5**, the intensity ratio of the $^5D_0 \rightarrow {}^7F_2/{}^5D_0 \rightarrow {}^7F_1$ transition is *ca.* 3.2, indicating that the site environment of the Eu^{III} ion in **5** is asymmetric, which is well coincident with the case that the Eu1 ion is coordinated by five oxygen atoms from two $[\alpha\text{-}SiW_{11}O_{39}]^{8-}$ subunits and three water ligands. Upon excitation at 320 nm, the as-synthesized solid of **7** yields four characteristic emission peaks of the Tb^{III} ions (Fig. 5c). These peaks are assigned to the $^5D_4 \rightarrow {}^7F_J$ (J = 6, 5, 4, 3) transitions, namely, $^5D_4 \rightarrow {}^7F_6$ (484 nm), $^5D_4 \rightarrow {}^7F_5$ (550 nm), $^5D_4 \rightarrow {}^7F_4$ (582 nm) and $^5D_4 \rightarrow {}^7F_3$ (630 nm), which are in good aggreement with previous research results.[50] The emission spectrum for **8** exhibits two bands at 488 and 585 nm upon excitation at 310 nm, which are attributed to the transitions of $^4D_{9/2} \rightarrow {}^6H_{15/2}$ and $^4D_{9/2} \rightarrow {}^6H_{13/2}$.[46] The mechanism of energy transfer from the ligand to the metal has been widely discussed to interpret the luminescence of lanthanide complexes.[51] In comparison with the emission spectra of **4**, **5**, **7** and **8**, the transition intensity changes in the order of $Eu^{III} > Tb^{III} \sim Dy^{III} > Sm^{III}$, which means that the ligand-to-metal charge transfer (LMCT) transitions of the Eu^{III}, Tb^{III}, Dy^{III} ions are more effective than those of the Sm^{III} ions.

Thermogravimetric analyses

The thermal stability of **2**, **3**, **5**, **6**, **7** and **8** has been investigated on crystalline samples under a N_2 atmosphere from 25 to 750 °C (Fig. S6).† Their thermogravimetric curves indicate two steps of weight loss. The first weight loss is 3.80% (calcd. 4.37%) from 25 to 288 °C, involving the release of 10 lattice water molecules and 6 coordination water molecules for **2**; 3.99% (calcd. 4.37%) from 25 to 288 °C, involving the release of 10 lattice water molecules and 6 coordination water molecules for **3**;. 3.95% (calcd. 4.36%) from 25 to 288 °C, involving the release of 10 lattice water molecules and 6 coordination water molecules for **5**;. 3.68% (calcd. 4.09%) from 25 to 288 °C, involving the release of 9 lattice water molecules and 6 coordination water molecules for **6**;. 3.80% (calcd. 4.37%) from 25 to 288 °C, involving the release of 8 lattice water molecules and 8 coordination water molecules for **7**; and 3.95% (calcd. 4.37%) from 25 to 288 °C, involving the release of 8 lattice water molecules and 8 coordination water molecules for **8**. The second weight loss is 7.29% (calcd. 7.83%) from 288 to 750 °C, approximately assigned to the removal of 2 coordination water molecules, 6 dap ligands and the dehydration of 4 protons for **2**; 7.23% (calcd. 7.83%) from 288 to 750 °C, approximately assigned to the decomposition of the removal of 2 coordination water molecules, 6 dap ligands and the dehydration of 4 protons for **3**; 7.37% (calcd. 7.81%) from 288 to 750 °C, approximately assigned to the decomposition of the removal of 2 coordination water molecules, 6 dap ligands and the dehydration of 4 protons for **5**; 7.30% (calcd. 7.82%) from 288 to 750 °C, approximately assigned to the decomposition of the removal of 2 coordination water molecules, 6 dap ligands and the dehydration of 4 protons for **6**; 6.86% (calcd. 7.29%) from 288 to 750 °C, approximately assigned to the decomposition of the removal of 6 dap ligands and the dehydration of 4 protons for **7** and 6.97% (calcd. 7.29%) from 288 to 750 °C, approximately assigned to the decomposition of the removal of 6 dap ligands and the dehydration of 4 protons for **8**. The observed experimental values are in approximate consistence with the theoretical values.

Conclusions

In conclusion, a class of unique 1-D double-chain organic–inorganic hybrid Cu–Ln heterometallic silicotungstates **1–9** have been hydrothermally synthesized and structurally characterized by elemental analyses, inductively coupled plasma atomic emission spectrometry, IR spectra, UV-Vis spectra, thermogravimetric analyses and single-crystal X-ray diffraction. X-Ray diffraction structural analyses indicate that **1–9** are isomorphic and adopt novel 1-D double-chain architectures formed by dimeric Cu–Ln heterometallic silicotungstate units by means of the bridging role of Ln cations. As far as we know, they exemplify a new type of organic–inorganic hybrid 1-D double-chain Cu–Ln heterometallic POMs. Moreover, the synthetic conditions of the reported silicotungstate-based TM–Ln heterometallic derivatives have been summarized. The magnetic properties of **2**, **3**, **6** and **8** have been measured. Furthermore, the luminescence properties of **4**, **5**, **7** and **8** have been examined and their luminescence behavior primarily originates from the nature of Ln cations. The thermal stability of **2**, **3**, **5**, **6**, **7** and **8** has been investigated. The successful isolations of **1–9** not only fertilize the structural chemistry of silicotungstates and promote the onging development of POM chemistry, but also provide an effective strategy for constructing other novel PTLHDs. We are currently investigating this domain using $K_8Na_2[A\text{-}\alpha\text{-}GeW_9O_{34}]\cdot 25H_2O$ in place of $Na_{10}[A\text{-}\alpha\text{-}SiW_9O_{34}]\cdot 18H_2O$. In the following work, (1) the N/O-containing functional ligands, variable TM cations and POM precursors will be introduced to our research system to obtain much more PTLHDs with

unexpected structures and properties; (2) chiral components will be employed in our system to control the charge distribution of microstructures of products, resulting in the noncoincidence of the centers for the positive and negative charges, and thus prepare ferroelectric, piezoelectric or nonlinear optical PTLHDs.

Acknowledgements

This work was supported by the Natural Science Foundation of China (21101055, 21071042, 21071043), China Postdoctoral Science Foundation Funded Project (201104392, 20100470996), the Natural Science Foundation of Henan Province (122300410106, 102300410093), the Foundation of State Key Laboratory of Structural Chemistry (20120013), 2012 Young Backbone Teachers Foundation from Henan Province, the Postdoctoral Science Foundation of Henan University (BH2010003), the Foundation of Education Department of Henan Province (2009A150003, 2010B150006) and the Students Innovative Pilot Plan of Henan University (2012).

References

1 (*a*) X. Fang, P. Kögerler, Y. Furukawa, M. Speldrich and M. Luban, *Angew. Chem., Int. Ed.*, 2011, **50**, 5212; (*b*) E. V. Chubarova, M. H. Dickman, B. Keita, L. Nadjo, F. Miserque, M. Mifsud, I. W. C. E. Arends and U. Kortz, *Angew. Chem., Int. Ed.*, 2008, **47**, 9542; (*c*) S. Gatard, S. Blanchard, B. Schollhorn, P. Gouzerh, A. Proust and K. Boubekeur, *Chem.–Eur. J.*, 2010, **16**, 8390; (*d*) J. Yan, J. Gao, D. L. Long, H. N. Miras and L. Cronin, *J. Am. Chem. Soc.*, 2010, **132**, 11410; (*e*) Z. M. Zhang, S. Yao, Y. G. Li, Y. H. Wang, Y. F. Qi and E. B. Wang, *Chem. Commun.*, 2008, 1650; (*f*) S. Z. Li, J. W. Zhao, P. T. Ma, J. Du, J. Y. Niu and J. P. Wang, *Inorg. Chem.*, 2009, **48**, 9819.

2 (*a*) P. Mialane, A. Dolbecq and F. Sécheresse, *Chem. Commun.*, 2006, 3477; (*b*) V. Lahootun, C. Besson, R. Villanneau, F. Villain, L. M. Chamoreau, K. Boubekeur, S. Blanchard, R. Thouvenot and A. Proust, *J. Am. Chem. Soc.*, 2007, **129**, 7127; (*c*) F. Hussain, B. S. Bassil, L. H. Bi, M. Reicke and U. Kortz, *Angew. Chem., Int. Ed.*, 2004, **43**, 3485; (*d*) L. J. Chen, D. Y. Shi, J. W. Zhao, Y. L. Wang, P. T. Ma, J. P. Wang and J. Y. Niu, *Cryst. Growth Des.*, 2011, **11**, 1913; (*e*) P. Mialane, A. Dolbecq, J. Marrot, E. Rivière and F. Sécheresse, *Chem.–Eur. J.*, 2005, **11**, 1771; (*f*) M. Sadakane, M. H. Dickman and M. T. Pope, *Angew. Chem., Int. Ed.*, 2000, **39**, 2914; (*g*) P. Mialane, L. Lisnard, A. Mallard, J. Marrot, E. Antic Fidancev, P. Aschehoug, D. Vivien and F. Sécheresse, *Inorg. Chem.*, 2003, **42**, 2102; (*h*) O. A. Kholdeeva, M. N. Timofeeva, G. M. Maksimov, R. I. Maksimovskaya, W. A. Neiwert and C. L. Hill, *Inorg. Chem.*, 2005, **44**, 666; (*i*) B. S. Bassil, M. H. Dickman, B. von der Kammer and U. Kortz, *Inorg. Chem.*, 2007, **46**, 2452; (*j*) J. W. Zhao, D. Y. Shi, L. J. Chen, X. M. Cai, Z. Q. Wang, P. T. Ma, J. P. Wang and J. Y. Niu, *CrystEngComm*, 2012, **14**, 2797.

3 A. Merca, A. Müller, J. V. Slageren, M. Läge and B. Krebs, *J. Cluster Sci.*, 2007, **18**, 711.

4 W. L. Chen, Y. G. Li, Y. H. Wang, E. B. Wang and Z. M. Zhang, *Dalton Trans.*, 2008, 865.

5 (*a*) X. K. Fang and P. Kögerler, *Angew. Chem., Int. Ed.*, 2008, **47**, 8123; (*b*) X. K. Fang and P. Kögerler, *Chem. Commun.*, 2008, 3396; (*c*) W. L. Chen, Y. G. Li, Y. H. Wang and E. B. Wang, *Eur. J. Inorg. Chem.*, 2007, 2216; (*d*) S. Yao, Z. M. Zhang, Y. G. Li, Y. Lu, E. B. Wang and Z. M. Su, *Cryst. Growth Des.*, 2010, **10**, 135; (*e*) Y. W. Li, Y. G. Li, Y. H. Wang, X. J. Feng, Y. Lu and E. B. Wang, *Inorg. Chem.*, 2009, **48**, 6452; (*f*) Z. M. Zhang, Y. G. Li, S. Yao and E. B. Wang, *Dalton Trans.*, 2011, **40**, 6475; (*g*) B. Nohra, P. Mialane, A. Dolbecq, E. Rivière, J. Marrot and F. Sécheresse, *Chem. Commun.*, 2009, 2703; (*h*) J. D. Compain, P. Mialane, A. Dolbecq, I. M. Mbomekallé, J. Marrot, F. Sécheresse, C. Duboc and E. Rivière, *Inorg. Chem.*, 2010, **49**, 2851; (*i*) J. F. Cao, S. X. Liu, R. G. Cao, L. H. Xie, Y. H. Ren, C. Y. Gao and L. Xu, *Dalton Trans.*, 2008, 115; (*j*) S. Reinoso and J. R. Galán-Mascarós, *Inorg. Chem.*, 2010, **49**, 377; (*k*) S. Reinoso, M. Giménez-Marqués, J. R. Galán-Mascarós, P. Vitoria and J. M. Gutiérrez-Zorrilla, *Angew. Chem., Int. Ed.*, 2010, **49**, 8384; (*l*) S. Reinoso, *Dalton Trans.*, 2011, **40**, 6610; (*m*) J. Y. Niu, S. W. Zhang, H. N. Chen, J. W. Zhao, P. T. Ma and J. P. Wang, *Cryst. Growth Des.*, 2011, **11**, 3769; (*n*) S. W. Zhang, Y. Wang, J. W. Zhao, P. T. Ma, J. P. Wang and J. Y. Niu, *Dalton Trans.*, 2012, **41**, 3764; (*o*) S. W. Zhang, J. W. Zhao, P. T. Ma, H. N. Chen, J. Y. Niu and J. P. Wang, *Cryst. Growth Des.*, 2012, **12**, 1263; (*p*) D. Y. Shi, J. W. Zhao, L. J. Chen, P. T. Ma, J. P. Wang and J. Y. Niu, *CrystEngComm*, 2012, **14**, 3108; (*q*) S. W. Zhang, J. W. Zhao, P. T. Ma, J. Y. Niu and J. P. Wang, *Chem.–Asian J.*, 2012, **7**, 966.

6 J. W. Zhao, C. M. Wang, J. Zhang, S. T. Zheng and G. Y. Yang, *Chem.–Eur. J.*, 2008, **14**, 9223.

7 (*a*) J. W. Zhao, J. Zhang, S. T. Zheng and G. Y. Yang, *Chem. Commun.*, 2008, 570; (*b*) H. Y. An, E. B. Wang, D. R. Xiao, Y. G. Li, Z. M. Su and L. Xu, *Angew. Chem., Int. Ed.*, 2006, **45**, 904.

8 (*a*) J. W. Zhao, H. P. Jia, J. Zhang, S. T. Zheng and G. Y. Yang, *Chem.–Eur. J.*, 2007, **13**, 10030; (*b*) J. Gopalakrishnan, *Chem. Mater.*, 1995, **7**, 1265; (*c*) D. Hagrman, C. Sangregorio, C. J. O'Connor and J. Zubieta, *J. Chem. Soc., Dalton Trans.*, 1998, 3707.

9 G. Hervé and A. Tézé, *Inorg. Chem.*, 1977, **16**, 2115.

10 G. M. Sheldrick, *SHELXL-97, Program for Crystal Structure Refinement*, University of Göttingen: Göttingen, Germany, 1997.

11 Z. M. Zhang, Y. G. Li, W. L. Chen, E. B. Wang and X. L. Wang, *Inorg. Chem. Commun.*, 2008, **11**, 879.

12 (*a*) D. Y. Shi, L. J. Chen, J. W. Zhao, Y. Wang, P. T. Ma and J. Y. Niu, *Inorg. Chem. Commun.*, 2011, **14**, 324; (*b*) L. J. Chen, D. Y. Shi, Y. Wang, H. L. Cheng, Z. D. Geng, J. W. Zhao, P. T. Ma and J. Y. Niu, *J. Coord. Chem.*, 2011, **64**, 400; (*c*) D. Y. Shi, Z. Q. Wang, J. J. Xing, Y. Y. Li, J. Luo, L. J. Chen and J. W. Zhao, *Synth. React. Inorg., Met.-Org., Nano-Met. Chem.*, 2012, **42**, 30.

13 (*a*) T. M. Anderson, W. A. Neiwert, K. I. Hardcastle and C. L. Hill, *Inorg. Chem.*, 2004, **43**, 7353; (*b*) N. Laronze, J. Marrot and G. Hervé, *Inorg. Chem.*, 2003, **42**, 5857; (*c*) L. H. Bi and U. Kortz, *Inorg. Chem.*, 2004, **43**, 7961; (*d*) B. S. Bassil, M. Ibrahim, R. Al-Oweini, M. Asano, Z. Wang, J. van Tol, N. S. Dalal, K. Y. Choi, R. N. Biboum, B. Keita, L. Nadjo and U. Kortz, *Angew. Chem., Int. Ed.*, 2011, **50**, 5961.

14 Crystal data of $[Cu(en)_2(H_2O)]_2[Cu(en)_2]_4[Si_2Cu_2W_{22}O_{78}]\cdot 7H_2O$: monoclinic, $P2_1/c$ space group, a = 18.811(2), b = 23.063(3), c = 26.039(4) Å, β = 96.267(3)°, V = 11230(3) Å^3, Z = 4, D_c = 3.987 g cm^{-3}, GOOF = 1.043, R_1 = 0.0775 and wR_2 = 0.1674.

15 (*a*) B. Li, J. W. Zhao, S. T. Zheng and G. Y. Yang, *Inorg. Chem.*, 2009, **48**, 8294; (*b*) J. W. Zhao, S. T. Zheng and G. Y. Yang, *J. Solid State Chem.*, 2008, **181**, 2205; (*c*) B. S. Bassil, S. Nellutla, U. Kortz, A. C. Stowe, J. van Tol, N. S. Dalal, B. Keita and L. Nadjo, *Inorg. Chem.*, 2005, **44**, 2659; (*d*) L. Lisnard, A. Dolbecq, P. Mialane, J. Marrot and F. Sécheresse, *Inorg. Chim. Acta*, 2004, **357**, 845.

16 I. D. Brown and D. Altermatt, *Acta Crystallogr., Sect. B: Struct. Sci.*, 1985, **41**, 244.

17 (*a*) Y. Q. Lan, S. L. Li, K. Z. Shao, X. L. Wang and Z. M. Su, *Dalton Trans.*, 2008, 3824; (*b*) D. Y. Du, J. S. Qin, S. L. Li, X. L. Wang, G. S. Yang, Y. G. Li, K. Z. Shao and Z. M. Su, *Inorg. Chim. Acta*, 2010, **363**, 3823.

18 R. D. Peacock and T. J. R. Weakley, *J. Chem. Soc. A*, 1971, 1836.

19 M. Sadakane, M. H. Dickman and M. T. Pope, *Angew. Chem., Int. Ed.*, 2000, **39**, 2914.

20 P. Mialane, L. Lisnard, A. Mallard, J. Marrot, E. Antic-Fidancev, P. Aschehoug, D. Vivien and F. Sécheresse, *Inorg. Chem.*, 2003, **42**, 2102.

21 P. Mialane, A. Dolbecq, E. Rivière, J. Marrot and F. Sécheresse, *Eur. J. Inorg. Chem.*, 2004, 33.

22 J. P. Wang, X. Y. Duan, X. D. Du and J. Y. Niu, *Cryst. Growth Des.*, 2006, **6**, 2266.

23 (*a*) E. Coronado and C. J. Gómez-García, *Chem. Rev.*, 1998, **98**, 273; (*b*) N. Mizuno andM., *Chem. Rev.*, 1998, **98**, 199; (*c*) P. Q. Zheng, Y. P. Ren, L. S. Long, R. B. Huang and L. S. Zheng, *Inorg. Chem.*, 2005, **44**, 1190.

24 C. Rocchiccioli-Deltcheff, M. Fournier, R. Franck and R. Thouvenot, *Inorg. Chem.*, 1983, **22**, 207.

25 C. Den Auwer, M. C. Charbonnel, M. G. B. Drew, M. Grigoriev, M.J. Hudson, B. P. Iveson, C. Madic, M. Nierlich, M. T. Presson, R. Revel, M. L. Russell and P. Thuery, *Inorg. Chem.*, 2000, **39**, 1487.

26 (*a*) S. Wang, Z. Pang, K. D. L. Smith and M. J. Wagner, *J. Chem. Soc., Dalton Trans.*, 1994, 955; (*b*) O. Kahn, *Adv. Inorg. Chem.*, 1995, **43**, 179; (*c*) A. C. Rizzi, R. Calvo, R. Baggio, M. T. Garland, O. Peña

and M. Perec, *Inorg. Chem.*, 2002, **41**, 5609; (*d*) O. Kahn, *Molecular Magnetism; VCH: Weinheim*, 1993.
27 (*a*) T. Sanada, T. Suzuki, T. Yoshida and S. Kaizaki, *Inorg. Chem.*, 1998, **37**, 4712; (*b*) R. E. P. Winpenny, *Chem. Soc. Rev.*, 1998, **27**, 447; (*c*) J. P. Costes, F. Dahan, A. Dupuis and J. P. Laurent, *Inorg. Chem.*, 1997, **36**, 3429; (*d*) A. Figuerola, J. Ribas, M. Llunell, D. Casanova, M. Maestro, S. Alvarez and C. Diaz, *Inorg. Chem.*, 2005, **44**, 6939; (*e*) M. Li, Y. Lan, A. M. Ako, W. Wernsdorfer, C. E. Anson, G. Buth, A. K. Powell, Z. Wang and S. Gao, *Inorg. Chem.*, 2010, **49**, 11587.
28 M. L. Kahn, J. Sutter, S. Golhen, P. Guionneau, L. Ouahab, O. Kahn and D. Chasseau, *J. Am. Chem. Soc.*, 2000, **122**, 3413.
29 Y. Li, F. K. Zheng, X. Liu, W. Q. Zou, G. C. Guo, C. Z. Lu and J. S. Huang, *Inorg. Chem.*, 2006, **45**, 6308.
30 C. Benelli and D. Gatteschi, *Chem. Rev.*, 2002, **102**, 2369.
31 (*a*) A. Furrer, H. U. Güdel, E. R. Krausz and H. Blank, *Phys. Rev. Lett.*, 1990, **64**, 68; (*b*) H. Lueken, P. Hannibal and K. Handrick, *J. Chem. Phys.*, 1990, **143**, 151; (*c*) J. P. Costes, F. Dahan, A. Dupuis and J. P. Laurent, *Chem.–Eur. J.*, 1998, **4**, 1616; (*d*) Z. H. Zhang, T. Okamura, Y. Hasegawa, H. Kawaguchi, L. Y. Kong, W. Y. Sun and N. Ueyama, *Inorg. Chem.*, 2005, **44**, 6219; (*e*) X. J. Zheng, C. Y. Sun, S. Z. Lu, F. H. Liao, S. Gao and L. P. Jin, *Eur. J. Inorg. Chem.*, 2004, 3262.
32 J. K. Tang, Y. Z. Li, Q. L. Wang, E. Q. Gao, D. Z. Liao, Z. H. Jiang, S. P. Yan, P. Cheng, L. F. Wang and G. L. Wang, *Inorg. Chem.*, 2002, **41**, 2188.
33 O. Kahn, *Molecular Magnetism*, VCH: Weinheim, 1993.
34 T. Peristeraki, M. Samios, M. Siczek, T. Lis and C. J. Milios, *Inorg. Chem.*, 2011, **50**, 5175.
35 H. Hou, G. Li, L. Li, Y. Zhu, X. Meng and Y. Fan, *Inorg. Chem.*, 2003, **42**, 428.
36 J. Y. Niu, K. H. Wang, H. N. Chen, J. W. Zhao, P. T. Ma, J. P. Wang, M. X. Li, Y. Bai and D. B. Dang, *Cryst. Growth Des.*, 2009, **9**, 4362.
37 F. He, M. L. Tong, X. L. Yu and X. M. Chen, *Inorg. Chem.*, 2005, **44**, 559.
38 O. Guillou, P. Bergerat, O. Kahn, E. Bakalbassis, K. Boubekeur, P. Batail and M. Guillot, *Inorg. Chem.*, 1992, **31**, 110.
39 (*a*) N. Ishikawa, M. Sugita, T. Okubo, N. Tanaka, T. Lino and Y. Kaizu, *Inorg. Chem.*, 2003, **42**, 2440; (*b*) C. Ritchie, M. Speldrich, R. W. Gable, L. Sorace, P. Kögerler and C. Boskovic, *Inorg. Chem.*, 2011, **50**, 7004; (*c*) K. C. Mondal, G. E. Kostakis, Y. Lan, W. Wernsdorfer, C. E. Anson and A. K. Powell, *Inorg. Chem.*, 2011, **50**, 11604; (*d*) J. Rinck, G. Novitchi, W. V. d. Heuvel, L. Ungur, Y. Lan, W. Wernsdorfer, C. E. Anson, L. F. Chibotaru and A. K. Powell, *Angew. Chem., Int. Ed.*, 2010, **49**, 7583; (*e*) M. L. Kahn, C. Mathonière and O. Kahn, *Inorg. Chem.*, 1999, **38**, 3692.
40 J. C. G. Buünzli and C. Piguet, *Chem. Soc. Rev.*, 2005, **34**, 1048.
41 G. J. Sopasis, M. Orfanoudaki, P. Zarmpas, A. Philippidis, M. Siczek, T. Lis, J. R. O'Brien and C. J. Milios, *Inorg. Chem.*, 2012, **51**, 1170.
42 C. Ritchie, V. Baslon, E. G. Moore, C. Reber and C. Boskovic, *Inorg. Chem.*, 2012, **51**, 1142.
43 (*a*) T. Yamase, *Chem. Rev.*, 1998, **98**, 307; (*b*) T. Yamase, T. Kobayashi, M. Sugeta and H. Naruke, *J. Phys. Chem. A*, 1997, **101**, 5046; (*c*) T. Ozeki and T. Yamase, *J. Alloys Compd.*, 1993, **192**, 28.
44 Y. G. Huang, B. L. Wu, D. Q. Yuan, Y. Q. Xu, F. L. Jiang and M. C. Hong, *Inorg. Chem.*, 2007, **46**, 1171.
45 A. Beeby, I. M. Clarkson, R. S. Dickins, S. Faulkner, D. Parker, L. Royle, A. S. de Sousa, J. A. G. Williams and M. Woods, *J. Chem. Soc., Perkin Trans. 2*, 1999, **3**, 493.
46 J. Xia, B. Zhao, H. S. Wang, W. Shi, Y. Ma, H. B. Song, P. Cheng, D. Z. Liao and S. P. Yan, *Inorg. Chem.*, 2007, **46**, 3450.
47 Q. H. Xu, L. S. Li, X. S. Liu and R. R. Xu, *Chem. Mater.*, 2002, **14**, 549.
48 (*a*) A. F. Kirby and F. S. Richardson, *J. Phys. Chem.*, 1983, **87**, 2544; (*b*) J. W. Stouwdam and F. C. J. M. van Veggel, *Nano Lett.*, 2002, **2**, 733; (*c*) Y. Su, L. Li and G. Li, *Chem. Mater.*, 2008, **20**, 6060.
49 T. Zhang, C. Spitz, M. Antonietti and C. F. J. Faul, *Chem.–Eur. J.*, 2005, **11**, 1001.
50 (*a*) C. A. Black, J. S. Costa, W. T. Fu, C. Massera, O. Roubeau, S. J. Teat, G. Aromí, P. Gamez and J. Reedijk, *Inorg. Chem.*, 2009, **48**, 1062; (*b*) Q. Gao, X. Wang and A. J. Jacobson, *Inorg. Chem.*, 2011, **50**, 9073.
51 (*a*) G. Stein and E. Wurzberg, *J. Chem. Phys.*, 1975, **62**, 208; (*b*) R. M. Supkowski, J. P. Bolender, W. D. Smith, L. E. L. Reynolds and W. D. Horrocks, *Coord. Chem. Rev.*, 1999, **185–186**, 307; (*c*) Z. H. Zhang, Y. Song, T. Okamura, Y. Hasegawa, W. Y. Sun and N. Ueyama, *Inorg. Chem.*, 2006, **45**, 2896.